

Diffusion on Ruffled Membrane Surfaces

Ali Naji

*Department of Physics, and Department of Chemistry and Biochemistry,
University of California, Santa Barbara, CA 93106*

Frank L. H. Brown

Department of Chemistry and Biochemistry, University of California, Santa Barbara, CA 93106

We present a position Langevin equation for overdamped particle motion on rough two-dimensional surfaces. A Brownian Dynamics algorithm is suggested to evolve this equation numerically, allowing for the prediction of effective (projected) diffusion coefficients over corrugated surfaces. In the case of static surface roughness, we find that a simple area-scaling prediction for the projected diffusion coefficient leads to seemingly quantitative agreement with numerical results. To study the effect of dynamic surface evolution on the diffusive process, we consider particle diffusion over a thermally fluctuating elastic membrane. Surface fluctuation has the effect of increasing the effective diffusivity toward a limiting annealed-surface value discussed previously. We argue that protein motion over cell surfaces spans a variety of physical regimes, making it impossible to identify a single approximation scheme appropriate to all measurements of interest.

I. INTRODUCTION

Diffusive processes are commonplace in many systems of chemical, physical and biological interest [1, 2, 3, 4], a fact commonly attributed to inherent randomness at the molecular level of dynamics (thermal or otherwise) and the wide range of applicability of the central limit theorem [4]. In the context of biological systems, diffusion plays a key role in many of the processes of life at the cellular and sub-cellular levels [2, 5]. In particular, the diffusion of molecules on the surface of cells has received widespread attention for many years [6, 7, 8, 9, 10], both due to the clear consequences this motion has for cellular functioning as well as the availability of suitable experimental techniques to make quantitative measurements. Developments in experimental techniques such as single-particle tracking [10], fluorescence photo-bleaching recovery [11] and nuclear magnetic resonance (NMR) [12] have made it possible to gain direct insight into the structure and dynamics of lipid membranes by investigating the lateral diffusion of lipids and integral membrane proteins [13].

Biological membranes are typically not flat, which leads to ambiguity in assigning the “diffusion coefficient” for a molecule on such a surface. Do we mean the intrinsic curvilinear diffusion coefficient, D_0 , that would be expected if the molecule were moving over a truly flat surface, or do we mean the effective diffusion coefficient, D , reflecting projected motion of the particle onto a reference plane (see Fig. 1)? Most experiments, including optical techniques and NMR [10, 11, 12], directly measure D , while traditional theories provide a route to estimation of D_0 [14, 15]. The connection between D and D_0 is the focus of this paper.

It is well appreciated that confining a particle to a two-dimensional (2D) surface within a three-dimensional (3D) space has the effect of lowering the effective diffusion coefficient, D , relative to the curvilinear value,

D_0 [16, 17, 18, 19, 20, 21, 22]. Recently, this geometric effect has seen renewed interest in the context of diffusion over lipid bilayers and biomembranes [23, 24, 25, 26]. Reflecting the diversity of membrane structures present in biology, some studies have focused interest on the case of a particle diffusing over a static membrane [16, 23, 26], while others have concentrated on membranes with fast dynamic fluctuations [24, 25]. For certain biological structures, the static membrane (quenched disorder) limit is probably a good one. For example, the endoplasmic reticulum (ER) [5] and the lateral cortex of auditory outer hair cells [27, 28] are oddly shaped in a predominantly static fashion due to topology of the membrane and interactions with other cellular components. Other systems, like reconstituted unilamellar vesicles [29] and the plasma membrane of the red blood cell [30] are expected to fluctuate rapidly, which motivated Reister and Seifert to consider the fast shape-fluctuation (annealed disorder) limit in the context of membrane protein diffusion [24]. The annealed disorder limit is especially attractive for theoretical study, since spatial correlations of the membrane surface drop out in this limit and analytical results are readily obtained [16]. More generally, membrane systems may fall in an intermediate regime where membrane motion and diffusive transport share comparable characteristic time scales.

While the annealed disorder limit is well understood, the opposite limit of quenched disorder is less established. One of the studies mentioned above [26] introduces an advanced computational strategy to analyze real experimental data for static configurations of ER membranes, but avoids detailed theoretical interpretation of the results. The static surface study by King [23], is plagued by an imprecise treatment of the diffusive process, which unfortunately leads to spurious results. Gustafsson and Halle [16] suggested a number of plausible approximations and rigorous bounds for the behavior of D over a static surface, and hypothesized that an effective medium approximation (EMA) [31] would provide the closest cor-

response with reality, but provided no direct evidence to support this conclusion.

Outside the field of biological physics, general simulation strategies have been suggested for the evolution of diffusive particles over curved surfaces of arbitrary complexity [18, 20]. While these methods can be applied to membrane systems, in many cases of interest they are more elaborate and computationally expensive than necessary. Commonly, biomembrane surfaces are described in the Monge gauge. The shape of the membrane surface is described by a single-valued function, $h(x, y)$, of lateral coordinates, x and y [32]; $h(x, y)$ provides the local height of the membrane above some arbitrary reference plane (see Fig. 1). Given this parameterization, it would seem natural to evolve the position of a particle in terms of its x and y coordinates, without direct consideration of the third dimension (excepting the implicit information found in $h(x, y)$).

This paper presents a 2D Langevin equation for diffusive particle motion over a curved Monge-gauge surface that may be static or fluctuating in time. The numerical implementation of this equation leads to simulations of increased efficiency relative to the more general 3D random-walk methodology of Holyst et al. [18]. Simulations are carried out here for surfaces with lateral periodicity.

In the quenched limit, simulation results for a variety of differently-shaped surfaces (periodic in a box of linear dimension L) suggest that the ratio between the projected and the curvilinear diffusion coefficients is equal to the ratio of projected membrane area, $\mathcal{A}_\perp = L^2$, to actual curvilinear membrane area, \mathcal{A} (to within the precision we are able to achieve numerically). That is, $D/D_0 \sim \mathcal{A}_\perp/\mathcal{A}$ for static Monge-gauge surfaces. These results directly refute an earlier claim of non-integer scaling with surface area [23] and disprove the suggestion [16] that the effective medium approximation should be the most accurate approximation available for predicting D from D_0 .

To examine the effects of dynamic surface fluctuations, we consider Helfrich elastic membranes with thermal dynamics described by a generalized continuum Langevin equation [8]. As a general trend, we show that the ratio D/D_0 grows with increasing membrane fluctuation rates. A particle moving on a slowly fluctuating membrane exhibits D approaching the quenched disorder limit discussed above, while fast membrane fluctuations effect D values limiting to the somewhat larger annealed limit results discussed previously [16, 24]. For a membrane of given rigidity, the crossover between these two regimes is controlled by a dimensionless parameter $\chi = k_B T / (4\eta L D_0)$, which represents the ratio between characteristic particle diffusion time and membrane shape-relaxation time scale in a hydrodynamic medium of viscosity η . A formal operator expansion in powers of χ^{-1} demonstrates the pre-averaging Fokker-Planck equation [24] as the limiting behavior associated with fast membrane fluctuations ($\chi^{-1} \rightarrow 0$). Additionally, this expansion suggests higher-order corrections, which may be of

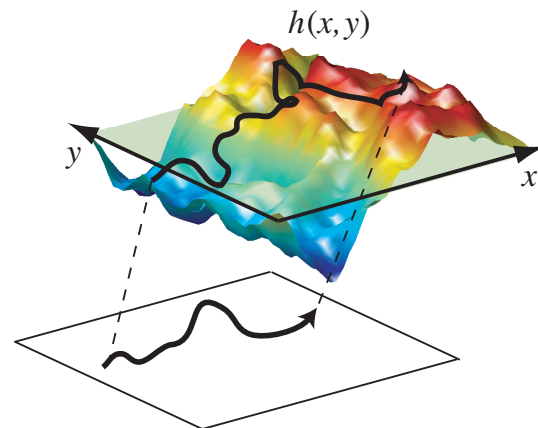


FIG. 1: A typical equilibrium configuration of a semiflexible elastic membrane described in Monge gauge. Projected self-diffusion in the $x - y$ plane (with effective diffusion coefficient D) is necessarily reduced relative to the curvilinear self-diffusion over the actual surface (with diffusion coefficient D_0) since any path followed on the membrane surface projects to a path of equal or smaller length in the base plane.

use in further theoretical study.

We consider a wide range of χ values in our simulations to fully characterize the transition between quenched and annealed regimes. Typical membrane proteins in sufficiently large tensionless biomembranes are expected to exhibit intermediate χ values, with D values falling in-between the quenched and annealed limits.

II. LANGEVIN EQUATION FOR DIFFUSION ON CURVED SURFACES

A. Membrane geometry

Let us briefly review some elementary geometric concepts of surfaces in order to introduce notation [33]. A curved 2D surface is parameterized by two independent coordinates. In the Monge gauge, one makes use of two Cartesian coordinates (x, y) with respect to a fixed frame in a 3D Euclidean space; in the absence of overhangs [32], $z = h(x, y)$ uniquely represents the membrane height from the $x - y$ plane (see Fig. 1). It is also convenient to define $\phi(\mathbf{r}) = z - h(x, y)$, to yield the surface equation in 3D: $\phi(\mathbf{r}) = 0$ where $\mathbf{r} = (x, y, z)$. The gradient vector, $\nabla_{\mathbf{r}}\phi = (-\partial_x h, -\partial_y h, 1)$, points normal to the surface with magnitude equal to the determinant of the surface metric

$$g = |\nabla_{\mathbf{r}}\phi|^2 = 1 + (\partial_x h)^2 + (\partial_y h)^2, \quad (1)$$

which formally determines the area rescaling of an infinitesimal surface element upon projection onto the $x - y$ plane, i.e.

$$d\mathcal{A} = \sqrt{g} d\mathcal{A}_\perp = \sqrt{g} dx dy, \quad (2)$$

where \mathcal{A} represents the curvilinear area of the surface and \mathcal{A}_\perp , the area projected on the $x - y$ plane.

Using a condensed notation $x_i = x, y$ for $i = 1, 2$, the metric tensor elements of the surface in the Monge gauge read

$$g_{ij} = \delta_{ij} + \partial_i h \partial_j h, \quad (3)$$

with δ_{ij} being the Kronecker delta and $\partial_i \equiv \partial/\partial x_i$ [34]. Hence one obtains the determinant $g = \det(\mathbf{g})$ and the inverse tensor

$$(\mathbf{g}^{-1})_{ij} = \delta_{ij} - \frac{\partial_i h \partial_j h}{g}. \quad (4)$$

Another useful quantity is the curvature tensor defined as [33]

$$K_{ij} = \frac{\partial_i \partial_j h}{\sqrt{g}} = -\frac{\partial_i \partial_j \phi}{\sqrt{g}}. \quad (5)$$

We will express some of our results in terms of the mean curvature,

$$H = \frac{1}{2}(\mathbf{g}^{-1})_{ij} K_{ij} \quad (6)$$

which gives the average of the two inverse principal radii of curvature at a given point on the surface. The Einstein summation convention is assumed above and in all that follows.

B. Discrete random walk on a membrane

Our goal is to establish a Langevin equation that describes the Brownian motion of a particle confined to $z = h(x, y)$. To this end, we first consider the case of discrete (but small) displacements over the membrane surface. Let us assume that a particle starts at \mathbf{r}_0 on the membrane surface (i.e., $\phi(\mathbf{r}_0) = 0$) before the discrete jump. A Brownian jump of finite duration Δt may be broken down into two consecutive steps [18] (see Fig. 2): i) The particle makes a random jump, $\Delta\boldsymbol{\zeta} = (\{\Delta\zeta_i\}, \Delta\zeta_z)$, to a new position $\mathbf{r}_1 = \mathbf{r}_0 + \Delta\boldsymbol{\zeta}$; this displacement is restricted to lie in the *local tangent plane* to the surface at \mathbf{r}_0 and is distributed according to a Gaussian probability distribution to be specified below. ii) The final location, $\mathbf{r}(\Delta t)$, of the particle is then obtained by an instantaneous normal projection of \mathbf{r}_1 back onto the membrane surface.

The net displacement of the particle, $\Delta\mathbf{r} \equiv \mathbf{r}(\Delta t) - \mathbf{r}_0$, may thus be written as

$$\Delta\mathbf{r} = \Delta\boldsymbol{\zeta} + \Delta_n \quad (7)$$

where the second term on the right hand side represents the normal projection (step ii), i.e.

$$\Delta_n \equiv \mathbf{r}(\Delta t) - \mathbf{r}_1 \simeq -\frac{\phi(\mathbf{r}_1) \nabla_{\mathbf{r}_1} \phi(\mathbf{r}_1)}{|\nabla_{\mathbf{r}_1} \phi(\mathbf{r}_1)|^2}, \quad (8)$$

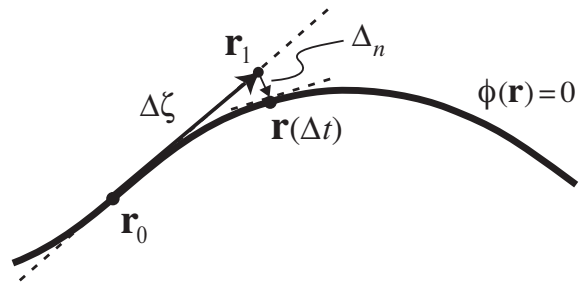


FIG. 2: Schematic representation of Eq. (7). Every discrete random-walk step (of duration Δt) over a curved surface (shown here by a thick curve for simplicity) may be broken down into two consecutive steps [18]. First, a random jump of size $\Delta\boldsymbol{\zeta}$ and duration Δt from the initial position \mathbf{r}_0 to a new position \mathbf{r}_1 in the local tangent plane (shown by dashed line). Second, an instantaneous normal-projection move of size Δ_n from \mathbf{r}_1 to the final location, $\mathbf{r}(\Delta t)$, on the surface. In the limit $\Delta t \rightarrow 0$, particle motion becomes exactly confined to the surface and, as shown in the text, may be describe by a well-defined Langevin equation. For the sake of representation, the jump size in the figure is exaggerated; note that Δ_n is perpendicular to both dashed tangent lines within the first order in $\Delta\boldsymbol{\zeta}$.

and for the first term we have

$$\Delta\boldsymbol{\zeta} \cdot \nabla_{\mathbf{r}_0} \phi(\mathbf{r}_0) = 0. \quad (9)$$

The above equations have been used to numerically simulate diffusion over a curved surface [18]. A significant merit of this methodology is that it may be used on arbitrarily shaped surfaces; i.e., a single-valued Monge-gauge parameterization is not required to implement this random-walk algorithm. In the case of a surface that may be specified by $h(x, y)$, this procedure may be simplified considerably, reducing the inherently 3D algorithm to a strictly 2D equation of motion, with the surface constraint $z = h(x, y)$ met exactly. (In contrast, the surface constraint is satisfied only to second order in jump size within the random-walk algorithm as implied by Eq. (8) [18].) This 2D equation of motion is specified in the following section.

Let us consider the second term in Eq. (7). For sufficiently small Δt , the length of the initial jump, $\Delta\boldsymbol{\zeta}$, becomes small enough to justify expanding $\phi(\mathbf{r}_1)$ around \mathbf{r}_0 . To second order in $\Delta\boldsymbol{\zeta}$,

$$\Delta_n \simeq -\frac{1}{2} [(\Delta\boldsymbol{\zeta} \cdot \nabla_{\mathbf{r}_0})^2 \phi(\mathbf{r}_0)] \frac{\nabla_{\mathbf{r}_0} \phi(\mathbf{r}_0)}{|\nabla_{\mathbf{r}_0} \phi(\mathbf{r}_0)|^2} + \mathcal{O}(\Delta\boldsymbol{\zeta}^3), \quad (10)$$

which shows that the projection displacement, Δ_n , is of the second order in the random jump size, $\Delta\boldsymbol{\zeta}$.

Using the notation introduced in Section II A, and rewriting this equation in Monge gauge, one finds the following set of equations

$$\Delta x_i = -\frac{1}{2} \left(\Delta\zeta_j \Delta\zeta_k \partial_j \partial_k h \right) \frac{\partial_i h}{g} \Big|_0 + \Delta\zeta_i + \mathcal{O}(\Delta\boldsymbol{\zeta}^3) \quad (11)$$

$$\Delta z = \frac{1}{2} \left(\Delta \zeta_j \Delta \zeta_k \partial_j \partial_k h \right) \frac{1}{g} \Big|_0 + \Delta \zeta_z + \mathcal{O}(\Delta \zeta^3). \quad (12)$$

Recall that $i, j, k = 1, 2$ denote only the projected $x - y$ components.

Note that in the first term on the right hand side of both equations, only the $x - y$ components of the random jump $\Delta \zeta$ enter. By virtue of Eq. (9), it follows that the z -component of the random jump, $\Delta \zeta_z = \Delta \zeta_i \partial_i h$, is not an independent variable. As a result, for sufficiently small time steps or random jumps, the displacement in the z direction, Δz , is fully described by the projected displacement in $x - y$ plane. In other words, Eq. (12) does not constitute an independent equation but merely a relation for the particle height variation, Δz , after each discrete step as enforced by the surface constraint $z = h(x, y)$. Indeed, one can easily check using Eqs. (11) and (9), that Δz is simply equal to the variation of the membrane height, Δh , for a small projected jump Δx_i , i.e.

$$\Delta z = \Delta h = \Delta x_i \partial_i h \Big|_0 + \frac{1}{2} \Delta x_i \Delta x_j \partial_i \partial_j h \Big|_0 + \dots, \quad (13)$$

where the right hand side is a Taylor expansion. Hence, in the limit of infinitesimal jumps, the particle is automatically confined to the surface as its $x - y$ position evolves according to Eq. (11).

C. Continuous time limit: Langevin equation

We now consider the time evolution relation (11) in the limit of infinitesimal time steps, that is formally $\Delta t \rightarrow dt$ or for the random jumps, $\Delta \zeta_i \rightarrow d\zeta_i$. The random jump was chosen so that it locally describes a free Brownian motion in the local tangent plane (characterized by a Gaussian distribution function) with a curvilinear diffusion coefficient D_0 and duration Δt . Thus, the projected jump probability density may be written as

$$P(\{\Delta \zeta_i\}) = \frac{\int d\mathbf{r} G_0(\mathbf{r}) \delta(z - x_i \partial_i h) \Pi_i \delta(\Delta \zeta_i - x_i)}{\int d\mathbf{r} G_0(\mathbf{r}) \delta(z - x_i \partial_i h)} \\ = \mathcal{N} \exp \left[-g_{ij} \Delta \zeta_i \Delta \zeta_j / (4D_0 \Delta t) \right], \quad (14)$$

where $G_0(x, y, z) = (4\pi D_0 \Delta t)^{-3/2} \exp[-\mathbf{r}^2 / 4D_0 \Delta t]$ is the usual Green's function for homogeneous 3D diffusion and the normalization is given by $\mathcal{N} = \sqrt{g} / (4\pi D_0 \Delta t)$. Formally, this distribution defines a generalized Wiener process [35], $\zeta_i(t)$, (with the non-constant kernel g_{ij}) in the base plane, whose properties are well-defined in the infinitesimal time-step limit; in particular, one has

$$d\zeta_i d\zeta_j = 2D_0 (\mathbf{g}^{-1})_{ij} dt, \quad (15)$$

and $d\zeta_i dt = 0$.

Rewriting Eq. (11) for an infinitesimal random jump, one thus obtains

$$dx_i = -D_0 \left[(\mathbf{g}^{-1})_{jk} \partial_j \partial_k h \right] \frac{\partial_i h}{g} dt + d\zeta_i. \quad (16)$$

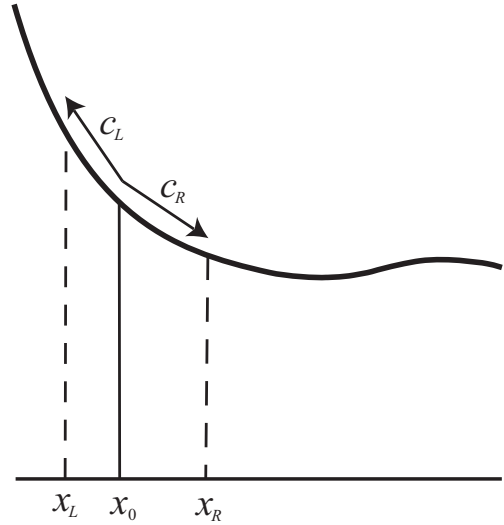


FIG. 3: Effect of curvature on the projected diffusive process: Curvature of a surface (here a line for simplicity) leads to deterministic drift within the Langevin equation. Two random steps of equal magnitude (c_L and c_R) cover the same curvilinear distance irrespective of direction, but translate into different projected distances ($|x_L - x_0|$ and $|x_R - x_0|$) due to surface shape. At a given position, the effect always favors displacement in the same direction, regardless of the exact (small) step size. Note that both slope and second derivative of the surface must be non-zero to break symmetry and drive the particle in a specific direction.

Note that the second-order term in random jump (coming from the projection displacement Δ_n) leads to a *drift*, which is of the order $\sim dt$, while the noise term scales as $d\zeta_i \sim dt^{1/2}$ and all higher-order terms formally vanish.

The corresponding Langevin equation immediately follows as

$$\dot{x}_i(t) = v_i + \tau_{ij} \eta_j(t), \quad (17)$$

where the drift term, $v_i = v_i[h(\{x_k(t)\})]$, reads

$$v_i = -D_0 \left[(\mathbf{g}^{-1})_{jk} \partial_j \partial_k h \right] \frac{\partial_i h}{g} = -2D_0 H \frac{\partial_i h}{\sqrt{g}}. \quad (18)$$

It is induced by the mean curvature, H , and local gradient of the surface. The fact that surface curvature drives local drift is easily understood in the context of diffusion on a 1D curved line (see Fig. 3). In the presence of curvature and non-vanishing slope, equidistant displacements in opposite directions along the curve necessarily lead to projected displacements of different magnitude.

In Eq. (17), we have defined $\tau_{ij} \eta_j(t) = d\zeta_i / dt$, where $\eta_i(t)$ is a Gaussian-distributed white noise of zero mean, $\langle \eta_i(t) \rangle = 0$, and variance

$$\langle \eta_i(t) \eta_j(t') \rangle = 2D_0 \delta_{ij} \delta(t - t'), \quad (19)$$

and $\tau_{ij} = \tau_{ij}[h(\{x_k(t)\})]$ is the square-root of the (positive-definite) inverse metric tensor, i.e.

$$(\mathbf{g}^{-1})_{ij} = \tau_{ik} \tau_{jk}. \quad (20)$$

The noise term in Eq. (17) is thus multiplied by a factor containing explicit dependence on (x, y) , a clear manifestation of “multiplicative noise” [4, 35]. The derivation we have presented suggests that the noise must be treated within the Ito prescription [4, 35]. The noise prefactor may be calculated by diagonalization of the inverse metric tensor as [36]

$$\tau_{ij} = \delta_{ij} - \frac{\partial_i h \partial_j h}{g + \sqrt{g}}. \quad (21)$$

This completes the derivation of the Langevin equation for free diffusion on a curved surface in Monge gauge.

The projected motion of a particle confined to a Monge-gauge surface may be regarded as formally equivalent to the motion of a particle in a 2D complex inhomogeneous environment characterized by an effective “potential”, $U(\{x_i\})$, and a locally varying diffusion matrix, $\mathcal{D}_{ij}(\{x_k\})$, both determined by the surface metric. The latter may be read off directly from the noise term as

$$\mathcal{D}_{ij} = D_0 (\mathbf{g}^{-1})_{ij}. \quad (22)$$

The explicit form of the effective potential may be seen more clearly from an equivalent Fokker-Planck equation [16]. Using methods described in [3, 35, 37], one can derive the following Fokker-Planck equation from the Langevin equation (17), i.e.

$$\partial_t \mathcal{P}(\{x_i\}, t) = D_0 \partial_i \left[\sqrt{g} (\mathbf{g}^{-1})_{ij} \partial_j \left(\frac{\mathcal{P}}{\sqrt{g}} \right) \right] \quad (23)$$

$$= \partial_i \left[\partial_j \left(\mathcal{D}_{ij} \mathcal{P} \right) - v_i \mathcal{P} \right] \quad (24)$$

$$= \partial_i \left[\mathcal{D}_{ij} \left(\partial_j \mathcal{P} - u_j \mathcal{P} \right) \right], \quad (25)$$

which governs the time evolution of the projected probability density, $\mathcal{P}(\{x_i\}, t)$, with the normalization condition $\int d^2x \mathcal{P}(\{x_i\}, t) = 1$. In the last equation, $u_j = -\partial_j U$ stands for the gradient of the effective dimensionless potential [16]

$$U(\{x_i\}) = -\frac{1}{2} \ln g. \quad (26)$$

III. DIFFUSION OVER A STATIC SURFACE

A. Brownian Dynamics simulations on a quenched surface

In order to demonstrate how the projected diffusion coefficient, D , is affected by static surface undulations, we consider diffusion over periodic surfaces $h(\{x_i + n_i L\}) = h(\{x_i\})$ with $i = 1, \dots, d$ in $d = 1$ and 2 surface dimensions and n_i being integers (hence, in 2D, the surface consists of identical square-like patches of size $L \times L$). This is

a convenient choice for numerical simulations, and allows for comparison with existing works.

The projected diffusion coefficient, D , is calculated by numerically evolving the projected position, $x_i(t)$, of a single particle (or equivalently, many non-interacting particles) according to the Langevin equation (17) and then evaluating

$$D = \lim_{t \rightarrow \infty} \frac{1}{2dt} \sum_{i=1}^d \overline{[x_i(t) - x_i(0)]^2}, \quad (27)$$

where the bar sign denotes average over an ensemble of particle trajectories with random initial conditions, $x_i(0)$ (as well as an ensemble of surface configurations in the case of the random surfaces introduced in Section III C 3). In all cases considered here, we choose surfaces (or ensembles of surfaces) with sufficient symmetry to insure that the principal directions x and y are equivalent. (The sum over i in Eq. (27) only serves to enhance sampling.)

In the simulations, we apply a standard iterative (Brownian Dynamics) algorithm [38] by discretizing the Langevin equation (17) using sufficiently small time steps of length δt . Hence at time $t = n \delta t$ (with integer $n \geq 0$),

$$x_i(n+1) = x_i(n) + v_i[x_k(n)] \delta t + \sqrt{2D_0 \delta t} \tau_{ij}[x_k(n)] w_j(n), \quad (28)$$

where w_i are Gaussian-distributed random numbers with zero mean, $\langle w_i(n) \rangle = 0$, and unit variance $\langle w_i(n) w_j(m) \rangle = \delta_{ij} \delta_{nm}$. This form of the discrete equation relies on the Ito interpretation of Eq. (17) previously mentioned. We emphasize that the lateral position of the particle is not constrained to any discrete lattice.

Within our level of description, the projected diffusion coefficient, D , must be linearly proportional to D_0 . This is because the only possible dimensional quantities affecting D are D_0 , L , and the surface shape, $h(x, y)$, and the only possible dimensionless quantity incorporating D_0 is the ratio D/D_0 , which must be expressible in terms of the other dimensionless quantities in the physical problem [39]. That is, $D/D_0 = f[h(x, y)/L]$ is a functional of the reduced surface shape alone (see also Section IV C 1). In the case of surfaces described by a single parameter, A (such as the amplitude in the sinusoidal and cycloid surfaces specified by Eqs. (35) and (36) below), D/D_0 is a function only of A/L .

In the quenched simulations, we typically employed a rescaled time step of $D_0 \delta t / L^2 \sim 10^{-6} - 10^{-5}$ and ran the simulations for approximately $10^6 - 10^7$ steps. It was verified that this choice of time step leads to convergence of the reported results for the roughest surfaces considered; i.e., further reduction of time step did not change the results within reported error-bars. Statistical averages are made over an ensemble of $5 \times 10^3 - 10^4$ trajectories (and membrane configurations where necessary) as discussed above. The error-bars are calculated using standard block-averaging methods [40]. Note that for a typical protein in a lipid bilayer, the diffusion coefficient $D_0 \sim 1 \mu\text{m}^2/\text{s}$. Assuming a membrane patch

of size $L \sim 0.1\mu\text{m}$, the simulation time steps fall in the range $\delta t \sim 0.01 - 1\mu\text{s}$.

We remark that simulations may also be done with the random-walk algorithm defined via Eqs. (7)-(9) as discussed in Ref. [18]. As we have shown in the previous Section, for sufficiently small time steps, this method is equivalent to the Langevin approach. The latter has the advantage that it implicitly constrains the particles to the membrane. Furthermore, it is a dynamical equation that may be generalized to study more complicated systems with, for instance, inter-particle or particle-membrane interactions. The random-walk algorithm is more convenient for surfaces with complicated geometry (such as 3D supramolecular assemblies) [18, 41], where the present Monge-gauge Langevin equation is not adequate. Also for surfaces with very large gradients, it is clear that the Langevin approach will eventually require smaller time steps than the 3D random-walk approach and thus longer computational runs. In practice, however, for the examples considered below, the Langevin simulations appear to be faster (typically by about 50% computer time in two dimensions) as compared with the random-walk algorithm. There are simply less computations per time step in the Langevin approach due to the analytical reduction of complexity when a Monge-gauge description is possible. Random-walk simulations were carried out on a number of the reported test-cases for comparison purposes—always with identical results to the Langevin simulations. For simplicity, these random-walk results are explicitly displayed only in Figure 4.

We will first consider numerics on simple periodic surfaces in one dimension where analytical results are available. We then progress to simple 2D surfaces (i.e., a sinusoidal surface and a crested cycloid [23]) and finally the case of an elastic membrane.

B. One dimension: exact result and simulations

In 1D, the local diffusion matrix (22) is a scalar and reads $\mathcal{D} = D_0/g$. Highly steep surface segments with large slopes relative to the x -axis ($g \gg 1$) represent regions with small local diffusion coefficient, $\mathcal{D}/D_0 \ll 1$, and large negative effective (dimensionless) potential, $-U \gg 1$, Eq. (26). Regions of high slope may be regarded as trapping potential wells (see also Fig. 8 below). Physically, the cause of this effect is clear. In regions of high slope, a particle which travels a large distance along the contour of the curve travels a relatively much smaller projected distance. The majority of travel is occurring in the z direction, not contributing to the projected diffusion coefficient, D .

The exact 1D expression for the projected diffusion coefficient along an arbitrary periodic curve may be written in terms of the metric determinant, $g = 1 + (\partial_x h)^2$, as

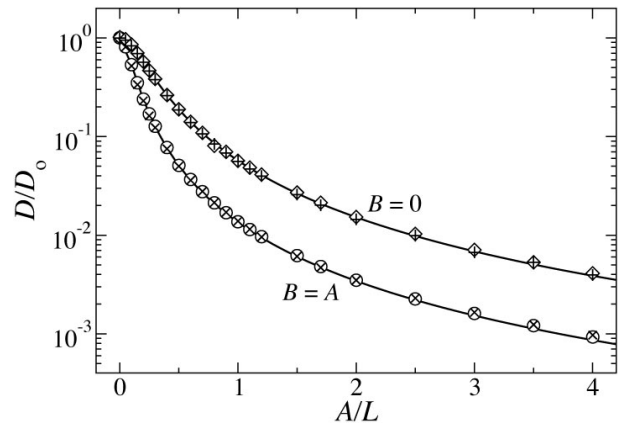


FIG. 4: Rescaled projected diffusion coefficient as a function of rescaled curve amplitude for free particle diffusion over a quenched 1D curve defined by Eq. (30) for two values of $B = 0$ and $B = A$ as indicated on the graph. Symbols show simulation data using Langevin dynamics (open diamonds and circles) and random-walk algorithm [18] (cross and plus symbols). The solid curves show the exact result, Eq. (29). Error-bars are smaller than the size of symbols.

[17, 21, 22]

$$\frac{D}{D_0} = \left(\frac{1}{L} \int_0^L dx \sqrt{g} \right)^{-2} = \left\langle \frac{1}{\sqrt{g}} \right\rangle^2 = \left(\frac{L}{L_c} \right)^2, \quad (29)$$

where brackets denote a contour average defined as $\langle \dots \rangle = \int_0^L dx \sqrt{g} (\dots) / \int_0^L dx \sqrt{g}$, and L_c is the contour length of the curve over a single projected period L .

It is not surprising that analytical results are available in 1D. The usual 1D Green's function for diffusion predicts statistically Gaussian behavior for motion along the contour length of the curve. For a Monge-gauge curve, this solution is readily transformed to the x -axis projected results, since contour length and projected length may be unambiguously mapped to one another. The projected solution in turn leads to Gaussian behavior in the long time limit with a simple rescaling by the square of the projected length to contour length ratio [17].

In Figure 4, we plot the Langevin simulations results (open symbols) for a quenched periodic curve defined as

$$h(x) = A \cos \frac{2\pi x}{L} + B \cos \frac{4\pi x}{L}. \quad (30)$$

for two different values of $B = 0$ and $B = A$. As seen, the numerical results exactly coincide with the analytical curve, Eq. (29), confirming thus the validity of the present Langevin approach. For comparison, we have also plotted in the Figure the simulation data (cross and plus symbols) obtained by applying the random-walk algorithm [18], Eqs. (7)-(9), which, as expected, coincide with both Langevin simulations data and exact results.

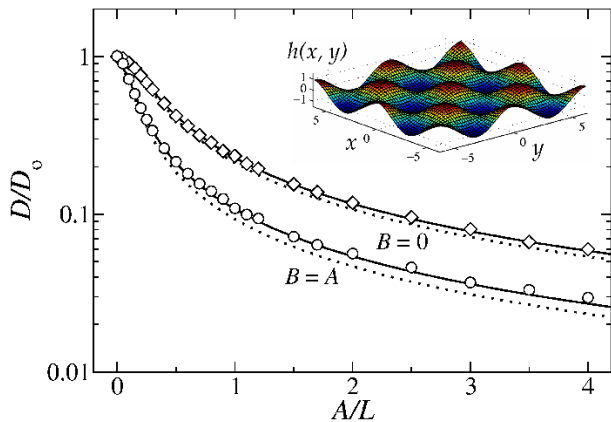


FIG. 5: Rescaled projected diffusion coefficient as a function of rescaled surface amplitude for free particle diffusion over a quenched surface defined by Eq. (35) for two values of $B = 0$ and $B = A$ as indicated on the graph. Symbols show Langevin simulation data (open diamonds and circles), while solid and dotted curves show the area-scaling and the effective medium predictions, Eqs. (34) and (33), respectively. Inset shows surface profile for $B = 0$, $A = 1$ and $L = 2\pi$. Error-bars are smaller than or equal to symbol size.

C. Diffusion on a 2D quenched manifold

Unlike the 1D problem, a rigorous result for the projected diffusion coefficient is not known for a quenched 2D surface. This relates to an intrinsic difference between Brownian motion on 1D and 2D manifolds [16]. Namely, on a 1D manifold, the distance between two points is given by the contour length which provides a natural parametrization, while on a 2D manifold, many different paths connect two given points, leading to analytical difficulties for establishing an exact result for a static surface [16, 17]. Nonetheless, several approximate results have been presented in the past that we shall briefly review below following the discussions by Gustafsson et al. [16].

1. Approximate analytical results

First, one may establish an upper bound and a lower bound that limit the admissible values for D using variational considerations [16, 21]. The result for the upper bound in the quenched surface limit reads [16]

$$\left. \frac{D}{D_0} \right|_{\text{upper}} = \frac{1}{2} \left(1 + \left\langle \frac{1}{g} \right\rangle \right), \quad (31)$$

where brackets denote a surface average defined as $\langle \dots \rangle = \int_0^L d^2x \sqrt{g} (\dots) / \int_0^L d^2x \sqrt{g}$.

Intuitively, one expects that the quenched 1D result, Eq. (29), establishes a lower bound since correlation effects induced by quenched surface undulations are ex-

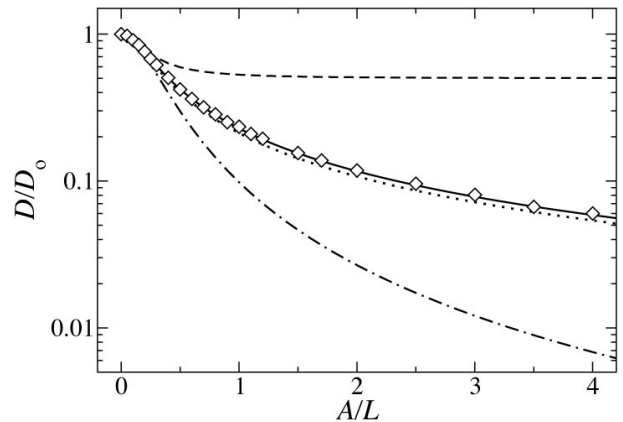


FIG. 6: Same as Fig. 5 but for $B = 0$. Symbols represent simulation data, dashed and dot-dashed curves are the predicted upper and lower bounds, Eqs. (31) and (32), and solid and dotted curves show the area-scaling prediction, Eq. (34), and the effective medium prediction, Eq. (33), respectively.

pected to be stronger in 1D [17]. Using variational methods, an expression similar to the 1D result may be obtained as [16]

$$\left. \frac{D}{D_0} \right|_{\text{lower}} = \frac{2\langle 1/\sqrt{g} \rangle^2}{1 + \langle 1/g \rangle}. \quad (32)$$

In addition to these variational bounds, a mean-field approach—referred to as effective medium approximation (EMA)—has been introduced [16, 31], which is supposed to provide a good approximation for projected diffusion coefficients on strongly disordered quenched surfaces, i.e.

$$\left. \frac{D}{D_0} \right|_{\text{EMA}} = \frac{1}{\langle \sqrt{g} \rangle}. \quad (33)$$

Finally, another plausible approximation for D can be deduced based on naive scaling arguments. On dimensional grounds, one might expect that an effective local isotropic projected diffusion coefficient would scale with the ratio of local projected area to actual curvilinear area, i.e., $D/D_0 \sim d\mathcal{A}_\perp/d\mathcal{A} = 1/\sqrt{g}$ (see Eq. (2)). Averaging this result over the entire surface leads to

$$\left. \frac{D}{D_0} \right|_{\text{area scaling}} = \left\langle \frac{1}{\sqrt{g}} \right\rangle = \frac{\mathcal{A}_\perp}{\mathcal{A}} \quad (34)$$

where the second equality follows from the definition of the averaging process as used in Eq. (31). One could have also guessed the second equality by applying similar arguments to the entire surface area instead of making local considerations. This conjecture finds some support in the fact that it is exact in 1D (see Eq. (29)). To our knowledge, no systematic derivation has been given so far in favor of the *area-scaling* prediction, though it has been discussed in several previous works [16, 23, 25].

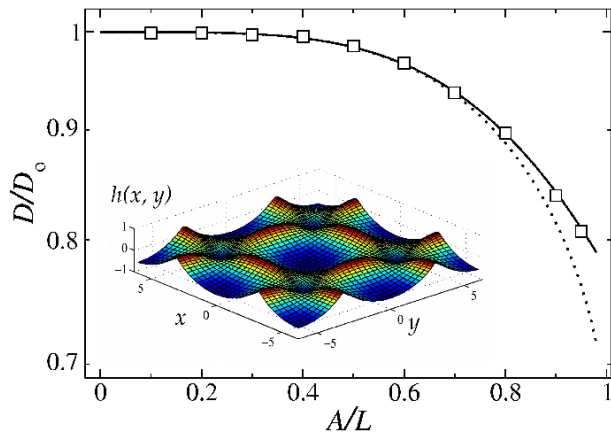


FIG. 7: Rescaled projected diffusion coefficient as a function of rescaled surface amplitude for free particle diffusion over a quenched crested cycloid defined by Eq. (36). Symbols show Langevin simulation data (open squares), and the solid and dotted curves show the area-scaling and the effective medium predictions, Eqs. (34) and (33), respectively. Inset shows the height profile of a cycloid with $L = 2\pi$ and $A = 0.7$. Error-bars are smaller than or equal to symbol size.

2. Simple periodic surfaces

In order to examine the aforementioned analytical approximations, we first consider a simple periodic surface defined as

$$h(x, y) = A \cos \frac{2\pi x}{L} \cos \frac{2\pi y}{L} + B \cos \frac{4\pi x}{L} \cos \frac{4\pi y}{L}. \quad (35)$$

Using Brownian Dynamics simulations as described in Section III A, we calculate the projected diffusion coefficient for two different cases with $B = 0$ and $B = A$ (shown by open symbols in Fig. 5). As seen, in both cases the simulation data for D/D_0 as a function of A/L agree well with the area-scaling prediction (solid curves). There are strong deviations from both upper and lower bounds as shown in Figure 6 (compare with dashed and dot-dashed curves, respectively). But for the above surface, the area-scaling result stays very close to the effective medium prediction (dotted curve). Note that for small A/L , the surfaces are nearly flat and different approximations work similarly well in this limit. Only in the large A/L limit, can one distinguish between different predictions. For $A/L \gg 1$, the upper bound value for D/D_0 tends to $1/2$, while the lower bound decays as $\sim (A/L)^{-2}$. The simulation data (as well as area-scaling and EMA predictions) fall off as $\sim (A/L)^{-1}$.

Next we consider diffusion on a crested cycloid defined

in a parametric form as

$$\begin{aligned} x &= u + \left(\frac{A}{2\pi}\right) \sin\left(\frac{2\pi u}{L}\right) \\ y &= v + \left(\frac{A}{2\pi}\right) \sin\left(\frac{2\pi v}{L}\right) \\ z &= -\frac{A^2}{2\pi L} \cos\left(\frac{2\pi u}{L}\right) \cos\left(\frac{2\pi v}{L}\right), \end{aligned} \quad (36)$$

where $z = h(x(u, v), y(u, v))$ represents the surface height (see Fig. 7 inset) and u and v are real numbers. Note that the cycloid is not single-valued for $A/L > 1$ and at $A/L = 1$, it shows singular cusp-like peaks. Therefore, we restrict our discussion to the range with $A/L < 1$. Diffusion on this surface was previously investigated in Ref. [23], where it was suggested that the projected diffusion coefficient deviates from the area-scaling prediction and follows the scaling law $D/D_0 = (\mathcal{A}_\perp/\mathcal{A})^{1.42}$.

In Figure 7, we have plotted the results from our simulations and compared with both the area-scaling and the effective medium approximation (solid and dotted curves, respectively). It is evident that the data closely follow the simple area-scaling rule $D/D_0 = (\mathcal{A}_\perp/\mathcal{A})$. In the present case, the area-scaling and effective medium curves diverge for growing A/L ratio, with the latter systematically underestimating the projected diffusion coefficient. The spurious results presented in Ref. [23] apparently stem from an incorrect treatment (neglect) of the surface metric within their simulation protocol.

3. Quenched elastic membrane

We now turn our attention to the case of a randomly undulated, quenched elastic membrane of size $L \times L$ with periodic boundary conditions. In the continuum limit (large length scales), we use the Helfrich membrane model with the Hamiltonian [43],

$$\begin{aligned} \mathcal{H} &= \frac{1}{2} \int_{\mathcal{A}_\perp} d\rho [K (\nabla_\rho^2 h)^2 + \sigma (\nabla_\rho h)^2] \\ &= \frac{1}{2L^2} \sum_{\mathbf{q}} \Omega_{\mathbf{q}} |h_{\mathbf{q}}|^2 \end{aligned} \quad (37)$$

where $\rho = (x, y)$, K is the bending rigidity, σ the surface tension, and

$$\Omega_{\mathbf{q}} = Kq^4 + \sigma q^2, \quad (38)$$

the energy spectrum of membrane fluctuations. For simplicity, we shall focus here only on two special cases, where only one of the elastic coefficients is non-zero.

At equilibrium, any configuration of the membrane may be viewed as a linear combination of several Fourier modes, $\mathbf{q} = (q_x, q_y)$, similar to Eq. (35) but with amplitudes, $h_{\mathbf{q}}$, distributed according to the Boltzmann weight $\sim \exp(-\mathcal{H}/k_B T)$. For numerical purposes, one needs

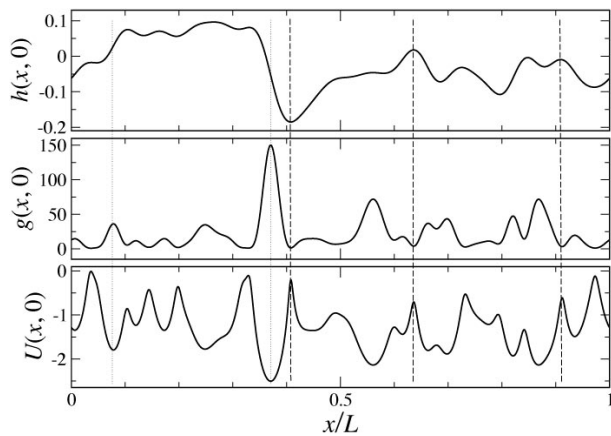


FIG. 8: Typical height profile, $h(x, y)$, metric determinant profile, $g(x, y)$, and effective (dimensionless) potential profile, $U(x, y)$, for an elastic membrane with bending rigidity $K/(k_B T) = 0.01$ and surface tension $\sigma = 0$ along the line $y = 0$. Vertical lines show typical regions with minimum (thin lines) and maximum (thick lines) potentials. As discussed in the text, these curves reflect a simple 1D slice through the surface. Consequently, non-perfect correlations are observed between, e.g., extrema in $h(x, 0)$, $g(x, 0)$ and $U(x, 0)$, reflecting the possibility of y -component contribution.

to introduce a small-scale cut-off, a (mimicking, for instance, a specific microscopic length scale) in order to filter the irrelevant short-wave-length modes. The height profile is still continuous and defined in space via

$$h(\boldsymbol{\rho}) = \frac{1}{L^2} \sum_{\mathbf{q}} h_{\mathbf{q}} e^{i\mathbf{q}\cdot\boldsymbol{\rho}}, \quad (39)$$

where $\mathbf{q} = (q_x, q_y) = (2\pi n, 2\pi m)/L$ with n, m being integral numbers in the range $-M/2 < n, m \leq M/2$ and $M = L/a$. In order to investigate diffusion over elastic membrane surfaces, we first numerically generate many equilibrium membrane configurations consistent with the above Hamiltonian by drawing $h_{\mathbf{q}}$ from normal distributions for each mode [42, 46] (see also Section IV).

We simulate the diffusion of a particle using the method described in Section III A, and average the mean-square displacement over an ensemble of $5 \times 10^3 - 10^4$ different equilibrium membrane configurations. As previously discussed, the rescaled projected diffusion coefficient, D/D_0 , is only a function of dimensionless membrane shape parameters, which, in the present case, are the rescaled bending rigidity $K/(k_B T)$, rescaled surface tension $\sigma a^2/(k_B T)$ and the ratio $M = L/a$ (see also Section IV C 1). Here we choose $M = 32$ for numerical convenience. (This choice is most sensible assuming a membrane patch of size $L \simeq 100$ nm, which implies a small-scale cut-off of $a \simeq 3$ nm, comparable to the size of lipid molecules.)

A typical membrane height profile along the $y = 0$ axis is shown for $\sigma = 0$ and $K/(k_B T) = 0.01$ in Figure 8 together with the profile of the surface metric determinant

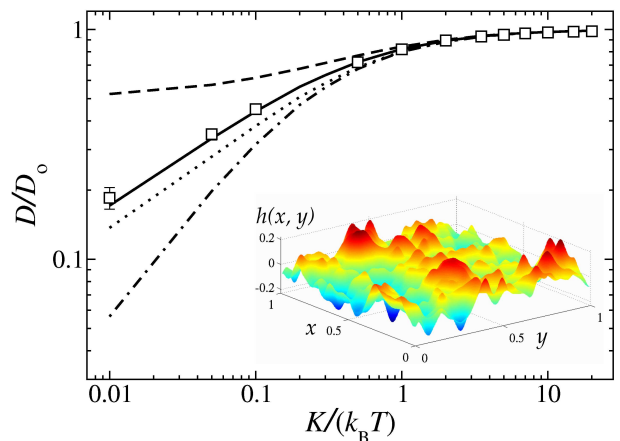


FIG. 9: Rescaled projected diffusion coefficient, D/D_0 , of a freely diffusing particle on a quenched ruffled membrane as a function of the rescaled membrane bending rigidity $K/(k_B T)$ for $M = 32$ and surface tension $\sigma = 0$. Symbols represent simulation data, the dashed curve is the upper bound, Eq. (31), the solid curve is the area-scaling prediction, Eq. (34), the dotted curve is the effective medium result, Eq. (33), and the dot-dashed curve shows the predicted lower bound, Eq. (32). Inset shows a typical membrane configuration with $K/(k_B T) = 0.01$, $L = 1$ and $M = 32$. Error-bars, if not shown, are smaller than or equal to the size of symbols.

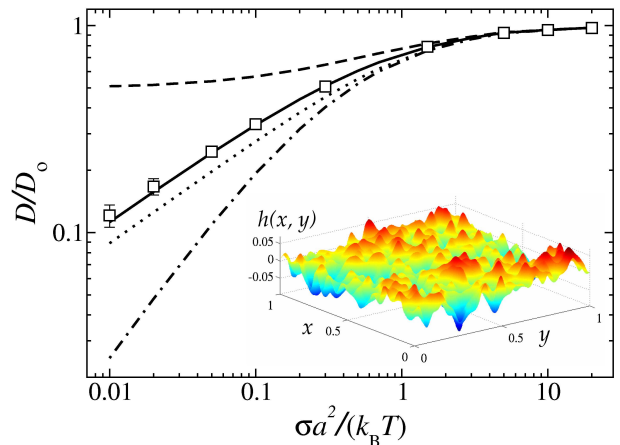


FIG. 10: Rescaled projected diffusion coefficient, D/D_0 , of a freely diffusing particle on a quenched ruffled membrane as a function of the rescaled membrane surface tension $\sigma a^2/(k_B T)$ for $M = 32$ and bending rigidity $K = 0$. Symbols represent simulation data, the dashed curve is the upper bound, Eq. (31), the solid curve is the area-scaling prediction, Eq. (34), the dotted curve is the effective medium result, Eq. (33), and the dot-dashed curve shows the predicted lower bound, Eq. (32). Inset shows a typical membrane configuration with $\sigma a^2/(k_B T) = 0.2$, $L = 1$ and $M = 32$. Error-bars, if not shown, are smaller than or equal to the size of symbols.

and the effective dimensionless potential, Eq. (26), experienced by a diffusing particle. Potential wells (peaks)

correspond to steep (flat) segments of the membrane and therefore a large (small) metric determinant as indicated by vertical lines on the graph. (Note that both x and y components of the surface gradient contribute to $g(x, 0)$ and $U(x, 0)$, and that only the x -component can explicitly be seen in $h(x, 0)$ plot in the Figure.)

The results for the disorder-averaged projected diffusion coefficient are plotted in Figure 9 as a function of the rescaled bending rigidity at fixed $\sigma = 0$ (open symbols) and in Figure 10 as a function of the rescaled surface tension at fixed $K = 0$. Both figures show qualitatively similar behavior for the simulation data and theoretical predictions. (It is to be noted that the theoretical curves are computed using Eqs. (31)-(34) and directly from the same ensemble of membrane configurations that are used in our Langevin simulations.) For large bending rigidities (or large surface tensions), the membrane stays close to a flat configuration and the data as well as all other theoretical predictions for D/D_0 tend to one (free planar diffusion) in the same manner. The difference between these results becomes pronounced and they can be distinguished in the limit of small bending rigidity (or small surface tension).

Interestingly, we find that in both cases the simulation data agree well with the area-scaling prediction (34) (shown by a solid curve) down to very small values of K and σ . In agreement with previous examples studied in this paper, the effective medium approximation (dotted curve) diverges from the simulation data for small K (or small σ) and, despite the suggestions made in Ref. [16], it represents a poorer approximation as compared to simple area scaling.

IV. DIFFUSION OVER A DYNAMICALLY FLUCTUATING SURFACE

So far we have only considered self-diffusion on a quenched surface. In this Section, we proceed by investigating dynamical effects from temporal surface fluctuations on the particle diffusion over a two-dimensional Monge-gauge membrane. As it turns out, the effects of membrane fluctuations on the projected diffusion coefficient can vary considerably depending on how fast membrane undulations relax relative to particle diffusion over the surface. In order to quantify this observation, one first needs to specify the dynamics of the surface.

A. Membrane dynamics

We shall adopt the Helfrich membrane model described by a continuum time-dependent height profile, $h(\boldsymbol{\rho}, t)$ with $\boldsymbol{\rho} = (x, y)$, whose equilibrium behavior may be determined by a Hamiltonian $\mathcal{H}[h(\boldsymbol{\rho})]$. As before, we assume periodic boundary conditions over a length scale of L in lateral directions. The dynamics of membrane height fluctuations in a low-Reynolds-number hydrody-

amic medium is customarily described by a Langevin-type equation [8, 44, 45],

$$\frac{\partial h(\boldsymbol{\rho}, t)}{\partial t} = \int_{-\infty}^{+\infty} d\boldsymbol{\rho}' \Lambda(\boldsymbol{\rho} - \boldsymbol{\rho}') [F(\boldsymbol{\rho}', t) + \eta(\boldsymbol{\rho}', t)], \quad (40)$$

where $\Lambda(\boldsymbol{\rho} - \boldsymbol{\rho}')$ is the hydrodynamic interaction specified by the Oseen tensor (a no-slip boundary condition on the impermeable membrane surface is assumed) [45, 46, 47],

$$\Lambda(\boldsymbol{\rho} - \boldsymbol{\rho}') = \frac{1}{8\pi\eta|\boldsymbol{\rho} - \boldsymbol{\rho}'|}, \quad (41)$$

$F(\boldsymbol{\rho}, t)$ is the force per unit area given by the functional derivative of the Hamiltonian,

$$F(\boldsymbol{\rho}, t) = -\frac{\delta\mathcal{H}}{\delta h(\boldsymbol{\rho}, t)}, \quad (42)$$

and $\eta(\boldsymbol{\rho}, t)$ is a spatially-varying Gaussian, white random force of zero mean, $\langle\eta(\boldsymbol{\rho}, t)\rangle = 0$, that satisfies the fluctuation-dissipation theorem

$$\langle\eta(\boldsymbol{\rho}, t)\eta(\boldsymbol{\rho}', t')\rangle = 2k_B T \Lambda^{-1}(\boldsymbol{\rho} - \boldsymbol{\rho}') \delta(t - t'). \quad (43)$$

This choice of noise clearly ensures that the membrane relaxes to equilibrium at long times.

To proceed, we express the membrane Langevin equation (40) in terms of Fourier modes $h_{\mathbf{q}}(t)$ with a discrete spectrum of wave-vectors $\mathbf{q} = (q_x, q_y) = (2\pi n, 2\pi m)/L$ where $-M/2 < n, m \leq M/2$ and $M = L/a$ as discussed in Section III C 3. Hence, we have

$$h(\boldsymbol{\rho}, t) = \frac{1}{L^2} \sum_{\mathbf{q}} h_{\mathbf{q}}(t) e^{i\mathbf{q}\cdot\boldsymbol{\rho}}, \quad (44)$$

using which we may write Eq. (40) as

$$\dot{h}_{\mathbf{q}}(t) = \Lambda_{\mathbf{q}} F_{\mathbf{q}}(t) + \sqrt{k_B T L^2 \Lambda_{\mathbf{q}}} \xi_{\mathbf{q}}(t), \quad (45)$$

where $F_{\mathbf{q}}(t)$ is the Fourier-transform of the force (42), $\Lambda_{\mathbf{q}} = 1/(4\eta q)$ is that of the Oseen interaction and $\xi_{\mathbf{q}}(t)$ is a redefined Gaussian white noise with $\langle\xi_{\mathbf{q}}(t)\rangle = 0$ and

$$\langle\xi_{\mathbf{q}}(t)\xi_{\mathbf{q}'}(t')\rangle = 2\delta_{\mathbf{q}, -\mathbf{q}'} \delta(t - t'). \quad (46)$$

It is understood that because $h(\boldsymbol{\rho}, t)$ is real, $h_{\mathbf{q}}(t)$ is a complex number with $h_{\mathbf{q}}^*(t) = h_{-\mathbf{q}}(t)$, guaranteeing that the number of independent Fourier modes remains M^2 .

Equation (45) introduces an efficient algorithm, known as Fourier-Space Brownian Dynamics method [42, 46], for simulating dynamics of biological membranes with arbitrary interaction potentials.

B. Coupled membrane-particle equations

In what follows, we shall focus on the case of a free elastic membrane described by the elastic Hamiltonian

(37). The force term in Eq. (45) thus simplifies to a linear form $F_{\mathbf{q}}(t) = -\Omega_{\mathbf{q}} h_{\mathbf{q}}(t)$, with $\Omega_{\mathbf{q}}$ defined in Eq. (38).

Putting together Eqs. (17) and (45), we have the following set of dynamical equations for free particle diffusion on a free Monge-gauge elastic membrane,

$$\dot{x}_i(t) = v_i + \tau_{ij} \eta_j(t), \quad (47)$$

$$\dot{h}_{\mathbf{q}}(t) = -\omega_{\mathbf{q}} h_{\mathbf{q}}(t) + \sqrt{k_B T L^2 \Lambda_{\mathbf{q}}} \xi_{\mathbf{q}}(t), \quad (48)$$

where the decay rates, $\omega_{\mathbf{q}}$, are defined as

$$\omega_{\mathbf{q}} = \Lambda_{\mathbf{q}} \Omega_{\mathbf{q}} = \Lambda_{\mathbf{q}} (K q^4 + \sigma q^2) \quad (49)$$

It is to be noted that the particle dynamics (via Eq. (47)) in the present description is *passive* in the sense that it does not influence dynamics of the membrane (see the Discussion). However, as the height profile modes evolve in time (via Eq. (48)), they directly influence the curvature-induced drift, v_i , and the multiplicative noise factor, τ_{ij} , which are related to the local height of the membrane in real space, $h(x, y, t)$, as discussed in Section II.

The free membrane equations (48) can be solved analytically as they correspond to a set of independent Ornstein-Uhlenbeck processes [4]. The time evolution of $h_{\mathbf{q}}(t)$ (starting from the initial value $h_{\mathbf{q}}^0 = h_{\mathbf{q}}(0)$), is governed by the conditional probability distribution

$$P(h_{\mathbf{q}}, t | h_{\mathbf{q}}^0, 0) = \sqrt{\frac{\beta \Omega_{\mathbf{q}}}{2\pi L^2 (1 - e^{-2\omega_{\mathbf{q}} t})}} \times \exp \left[-\frac{\beta \Omega_{\mathbf{q}}}{2L^2} \frac{|h_{\mathbf{q}} - h_{\mathbf{q}}^0 e^{-\omega_{\mathbf{q}} t}|^2}{1 - e^{-2\omega_{\mathbf{q}} t}} \right]. \quad (50)$$

C. Crossover from quenched to annealed disorder limit

In general, the coupled dynamical equations (47) and (48) can be used to study the diffusion process on a surface that may be static, as studied in previous Sections, or dynamic. The quenched disorder as well as the annealed disorder limits can thus be realized as special cases of Eqs. (47) and (48), by choosing the membrane-related parameters (such as bending rigidity or medium viscosity) such that the membrane decay rates, $\omega_{\mathbf{q}}$, tend to zero (static surface) or infinity (fast-fluctuating surface). Physically, however, these same limits can also be achieved by taking a very large or small curvilinear particle diffusion coefficient, D_0 . The coupling between particle and membrane motions introduces a new dimensionless parameter to the problem not present in the quenched case (or the annealed case). This parameter can be used to track the transition from quenched to annealed limits.

1. Reduced representation

In order to demonstrate this feature, we shall use a reduced (dimensionless) representation by rescaling length and time scales by a characteristic length and time, that is, using $\tilde{x} = x/L$, or equivalently, $\tilde{\mathbf{q}} = \mathbf{q}L$, $\tilde{t} = D_0 t/L^2$, as well as $\tilde{h}(\tilde{x}, \tilde{y}, \tilde{t}) = h(x, y, t)/L$, or equivalently, $\tilde{h}_{\tilde{\mathbf{q}}}(\tilde{t}) = h_{\mathbf{q}}(t)/L^3$. Hence we obtain

$$\dot{\tilde{x}}_i(\tilde{t}) = \tilde{v}_i + \tilde{\tau}_{ij} \tilde{\eta}_j(\tilde{t}), \quad (51)$$

$$\dot{\tilde{h}}_{\tilde{\mathbf{q}}}(\tilde{t}) = -\chi \tilde{\omega}_{\tilde{\mathbf{q}}} \tilde{h}_{\tilde{\mathbf{q}}}(\tilde{t}) + \sqrt{\chi \tilde{\Lambda}_{\tilde{\mathbf{q}}}} \tilde{\xi}_{\tilde{\mathbf{q}}}(\tilde{t}), \quad (52)$$

where the rescaled functions, namely, rescaled drift, \tilde{v}_i , rescaled multiplicative noise factor, $\tilde{\tau}_{ij}$, as well as rescaled noise terms $\tilde{\eta}_i(\tilde{t})$ and $\tilde{\xi}_{\tilde{\mathbf{q}}}(\tilde{t})$, whose explicit forms are given in Appendix A, are independent of system parameters. The rescaled decay rate reads $\tilde{\omega}_{\tilde{\mathbf{q}}} = \tilde{\Lambda}_{\tilde{\mathbf{q}}} \tilde{\Omega}_{\tilde{\mathbf{q}}}$ where $\tilde{\Omega}_{\tilde{\mathbf{q}}} = \tilde{K} \tilde{q}^4 + \tilde{\sigma} \tilde{q}^2$ and $\tilde{\Lambda}_{\tilde{\mathbf{q}}} = 1/\tilde{q}$.

Note that all physical system parameters have been condensed into four dimensionless combinations. These are the rescaled bending rigidity $\tilde{K} = K/(k_B T)$, rescaled surface tension $\tilde{\sigma} = \sigma L^2/(k_B T)$, $M = L/a$, and an additional parameter

$$\chi = \frac{k_B T}{4\eta D_0 L}, \quad (53)$$

which we shall refer to as the *dynamical coupling parameter* as it embeds in itself the dynamical coupling between equations (47) and (48). Indeed, for vanishing dynamical coupling parameter $\chi \rightarrow 0$, the membrane equation reduces to $\dot{h}_{\mathbf{q}}(t) = 0$, representing a static surface.

One may also examine the conditional probability in rescaled units

$$\tilde{P}(\tilde{h}_{\tilde{\mathbf{q}}}, \tilde{t} | \tilde{h}_{\tilde{\mathbf{q}}}^0, 0) = \sqrt{\frac{\tilde{\Omega}_{\tilde{\mathbf{q}}}}{2\pi (1 - e^{-2\chi \tilde{\omega}_{\tilde{\mathbf{q}}} \tilde{t}})}} \times \exp \left[-\frac{\tilde{\Omega}_{\tilde{\mathbf{q}}}}{2} \frac{|\tilde{h}_{\tilde{\mathbf{q}}} - \tilde{h}_{\tilde{\mathbf{q}}}^0 e^{-\chi \tilde{\omega}_{\tilde{\mathbf{q}}} \tilde{t}}|^2}{1 - e^{-2\chi \tilde{\omega}_{\tilde{\mathbf{q}}} \tilde{t}}} \right], \quad (54)$$

which is defined via $\tilde{P}(\tilde{h}_{\tilde{\mathbf{q}}}, \tilde{t} | \tilde{h}_{\tilde{\mathbf{q}}}^0, 0) = P(h_{\mathbf{q}}, t | h_{\mathbf{q}}^0, 0) L^3$. For $\chi \rightarrow 0$, the static surface solution is recovered, that is $\tilde{P}(\tilde{h}_{\tilde{\mathbf{q}}}, \tilde{t} | \tilde{h}_{\tilde{\mathbf{q}}}^0, 0) \rightarrow \delta(\tilde{h}_{\tilde{\mathbf{q}}} - \tilde{h}_{\tilde{\mathbf{q}}}^0)$, while for $\chi \rightarrow \infty$, it rapidly decays to the equilibrium distribution

$$\tilde{P}(\tilde{h}_{\tilde{\mathbf{q}}}, \tilde{t} | \tilde{h}_{\tilde{\mathbf{q}}}^0, 0) \rightarrow \tilde{P}_{\text{eq}}(\tilde{h}_{\tilde{\mathbf{q}}}) = \left(\frac{\tilde{\Omega}_{\tilde{\mathbf{q}}}}{2\pi} \right)^{1/2} e^{-\tilde{\Omega}_{\tilde{\mathbf{q}}} |\tilde{h}_{\tilde{\mathbf{q}}}|^2/2}. \quad (55)$$

These two limits therefore reflect the static surface (quenched disorder) and the fast-fluctuating surface (annealed disorder) limits, respectively. Solving the set of equations (51) and (52) for a finite intermediate value of χ allows one to investigate the *intermediate regime*, as we shall do later.

The reduced representation explicitly demonstrates that any dimensionless quantity obtained via simulations must depend on individual system parameters *only*

through the dimensionless combinations \tilde{K} , $\tilde{\sigma}$, χ , and $M = L/a$. This implies that the ratio of the projected diffusion coefficient and the curvilinear diffusion coefficient, D/D_0 , has the general form

$$\frac{D}{D_0} = f(\tilde{K}, \tilde{\sigma}, \chi, M), \quad (56)$$

which could be surmised simply from dimensional considerations [39]. From a practical perspective, the reduced approach simplifies our investigation of the dependence of D/D_0 on various system parameters. The addition of membrane motion adds only a single dimensionless parameter beyond those necessary in describing the quenched limit. This parameter, χ , may be thought of as a rescaled solvent viscosity. Since χ appears only when surface dynamics is important, we tend to focus attention on it when calculating D/D_0 over fluctuating surfaces. However, we stress that all the dimensionless parameters of the system influence the value of D/D_0 .

Another advantage of the reduced representation is that it immediately suggests a ‘‘small parameter’’ for use in a perturbative expansion around the analytical annealed limit results. In Appendix C, we present an operator expansion in powers of χ^{-1} . At zeroth order, the pre-averaging Fokker-Planck equation of Reister and Seifert [24] is recovered. Higher-order corrections are predicted, but not pursued in this work.

2. Characteristic time scales

The physical meaning of the dynamical coupling parameter, χ , may be appreciated further when looking at the typical time scales that characterize the dynamics of particle diffusion and that of membrane relaxation.

The typical diffusion time over a length of size q^{-1} may be written as $\tau_{\mathbf{q}}^d = 1/(D_0 q^2)$, while the relaxation time of an undulation of wave-length q^{-1} is given by $\tau_{\mathbf{q}}^m = \omega_{\mathbf{q}}^{-1}$. Using the definition of the decay rate, $\omega_{\mathbf{q}}$, we have the time scale ratio

$$\frac{\tau_{\mathbf{q}}^d}{\tau_{\mathbf{q}}^m} = \frac{Kq^2 + \sigma}{4\eta D_0 q} = \chi \left(\frac{\tilde{K}\tilde{q}^2 + \tilde{\sigma}}{\tilde{q}} \right). \quad (57)$$

In general, one can define the quenched disorder limit as the limit where the membrane relaxation time becomes much larger than the diffusion time. While, the converse limit of vanishingly small relaxation time represents the annealed disorder limit. When the two time scales are comparable, one encounters an intermediate situation.

Clearly, at short wave-lengths $q \rightarrow \infty$, one always deals with an annealed situation. But it is the long wave-length, $q \rightarrow 0$, behavior which is of primary practical importance in the context of physical measurements. A membrane with a finite surface tension always exhibits annealed behavior at sufficiently long wave-lengths as seen from Eq. (57), whereas a membrane with only

bending rigidity exhibits quenched behavior at long wave-lengths.

It is evident that in a *finite* or *periodic* system, such as the ones considered in this paper where the wave-vector is bounded from below by the surface periodicity $q > 2\pi/L$, the transition from one limit to another can be established theoretically by changing the dynamical coupling parameter over the range $0 \leq \chi < \infty$ at fixed bending rigidity, surface tension and M . This is indicated by the second equality in Eq. (57). In what follows, we shall focus only on the case with zero surface tension, $\sigma = 0$, where quenched behavior can be achieved within reasonable values for system parameters.

D. Coupled particle-membrane simulation method

In order to simulate diffusion on a dynamic surface in an arbitrary dynamical situation, we apply the standard Brownian Dynamics algorithm by discretizing the time into steps of sufficiently small length similar to what we described in Section III A. In order to bring up the role of the dynamical coupling and provide a unified analysis of the quenched-annealed crossover behavior, it is most convenient to simulate the system in the reduced representation using Eqs. (51) and (52), where all various system parameters condense into a few relevant dimensionless parameters.

We evolve particle position using small rescaled time steps $\delta\tilde{t}$ such that at time $\tilde{t} = n\delta\tilde{t}$ (with $n \geq 0$ being an integer)

$$\tilde{x}_i(n+1) = \tilde{x}_i(n) + \tilde{v}_i(n)\delta\tilde{t} + \sqrt{2\delta\tilde{t}}\tilde{\tau}_{ij}(n)w_j(n) \quad (58)$$

for $i, j = 1, 2$, where w_i are Gaussian-distributed random numbers with zero mean, $\langle w_i(n) \rangle = 0$, and unit variance $\langle w_i(n)w_j(m) \rangle = \delta_{ij}\delta_{nm}$. Other rescaled functions appearing in the above equation are given explicitly in Appendix A. They are evaluated from the instantaneous membrane height $\tilde{h}(\{\tilde{x}_i(n)\}, n) = \tilde{h}(\tilde{x}(n), \tilde{y}(n), n)$ obtained from the Fourier modes $\tilde{h}_{\tilde{\mathbf{q}}}(n)$, via Eq. (44).

Note that to evaluate $\tilde{h}_{\tilde{\mathbf{q}}}$ at each time step, one can either use the discretized form of Eq. (52), i.e.

$$\tilde{h}_{\tilde{\mathbf{q}}}(n+1) = \tilde{h}_{\tilde{\mathbf{q}}}(n) - \chi\tilde{\omega}_{\tilde{\mathbf{q}}}\tilde{h}_{\tilde{\mathbf{q}}}(n)\delta\tilde{t} + \sqrt{\chi\tilde{\Lambda}_{\tilde{\mathbf{q}}}\delta\tilde{t}}\tilde{R}_{\tilde{\mathbf{q}}}(n), \quad (59)$$

(with random complex variables $\tilde{R}_{\tilde{\mathbf{q}}}$ of zero mean and variance $\langle \tilde{R}_{\tilde{\mathbf{q}}}(n)\tilde{R}_{\tilde{\mathbf{q}}'}(m) \rangle = 2\delta_{\tilde{\mathbf{q}}, -\tilde{\mathbf{q}}'}\delta_{nm}$), or directly draw $\tilde{h}_{\tilde{\mathbf{q}}}(n)$ values from the Ornstein-Uhlenbeck Gaussian distribution, Eq. (54). The second method has the clear advantage that it is based on an exact result and is computationally easier to implement as previously performed in Ref. [42]. We have used both methods in our simulations with the same results obtained within the statistical error-bars.

The time step $\delta\tilde{t}$ must be chosen such that it ensures the convergence of Eq. (58) (and Eq. (59), if applied).

Even if the membrane dynamics are drawn from the exact distribution (54), care must still be taken to insure that a small enough $\delta\tilde{t}$ is used to properly capture the effect of membrane dynamics in Eq. (58). Both the drift and diffusion tensor for the particle depend upon the local height of the membrane and it is to be expected that at large χ , one needs to use time steps limited by the membrane dynamics as opposed to particle diffusion. We typically choose rescaled time steps in the range $\delta\tilde{t} = 10^{-8} - 10^{-6}$, and run the simulations for $10^5 - 10^7$ time steps. (As indicated previously, step size is verified by checking for convergence of results.) In the simulations, we measure the projected diffusion coefficient via the mean square displacement of a Brownian particle as defined in Eq. (27). (Simulated mean square displacements converge more quickly with time to a diffusive long-time behavior for large χ or highly fluctuating membranes.) We average the results over an ensemble of $5 \times 10^3 - 10^4$ particle trajectories with random initial conditions for the particle as well as the membrane height profile.

In our simulations, the coupling parameter is varied over the range $\chi = 10^{-4} - 10^2$ and the rescaled membrane bending rigidity in the range $\bar{K} = 0.01 - 10$, with $M = L/a = 32$ being chosen as in the quenched study in Section III C 3. Recall that at fixed bending rigidity and system size, changing $\chi = k_B T / (4\eta D_0 L)$ may be viewed as changing either the curvilinear diffusion coefficient, D_0 , or the medium viscosity, η , or a combination of both. They all have the same quantitative effect on D/D_0 , once \bar{K} and M are fixed.

E. Simulation results

In Figure 11, we show simulation results for the ratio of the projected diffusion coefficient to the curvilinear diffusion coefficient, D/D_0 , as a function of the membrane bending rigidity with a number of different values chosen for the dynamical coupling parameter, χ . The case of $\chi = 0$ (filled squares) represents a strictly quenched membrane, with results reproduced from Section III C 3. As mentioned before, the quenched data agree with the area-scaling prediction (solid curve). (In the Figure, we use a log-log plot and explore bending rigidities down to very small (unphysical for lipid bilayers) values to clearly display the predicted trends. At large K , both quenched and annealed results converge to within just a few percent.)

It is clearly seen that, as the dynamical coupling parameter increases, the projected diffusion coefficient deviates from and becomes larger than its quenched value, indicating that dynamical fluctuations of the surface enhance particle diffusion. This is to be expected based on very general considerations that imply fast surface fluctuations help to excite the particle through potential barriers more easily as it moves over the surface [16]. For larger values of χ (stronger surface fluctuations), the data tend to the theoretical annealed prediction (shown by a

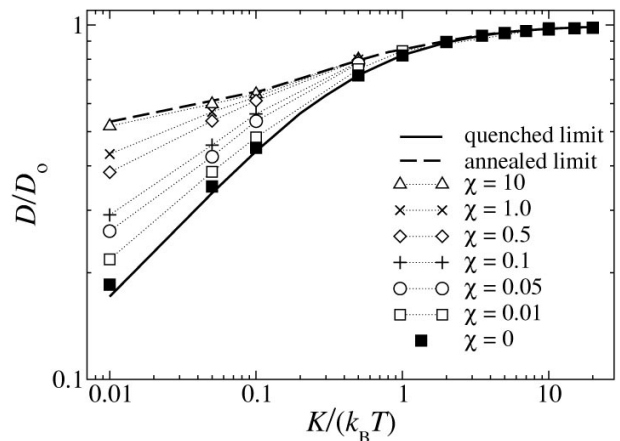


FIG. 11: Rescaled projected diffusion coefficient, D/D_0 , of a freely diffusing particle on a dynamically fluctuating elastic membrane as a function of the rescaled membrane bending rigidity $K/(k_B T)$ for $M = 32$ and surface tension $\sigma = 0$. Symbols represent simulation data for various dynamical coupling parameters, χ , spanning the whole intermediate dynamical coupling regime from quenched membrane limit with $\chi = 0$ (filled squares, same data as in Figure 9) to a rapidly fluctuating membrane with $\chi = 10$ (open triangle-ups). The dashed curve is the annealed theoretical prediction (as calculated in Appendix B), while the solid curve is the quenched area-scaling prediction, Eq. (34). Dotted lines are guide to eyes. Error-bars are removed for clarity (they are typically about the symbol size and comparable to or smaller than those shown in Fig. 9).

dashed curve in Figure 11) exhibiting a reasonably good quantitative agreement for $\chi > 10$ (see below). The calculation of the annealed curve is presented in Appendix B. It slightly differs from the approximate analytical results previously obtained in Refs. [16, 24] as we explain in the Appendix.

In order to examine the crossover behavior from the quenched to annealed disorder limit, we show in Figure 12 the simulated diffusion coefficients as a function of the dynamical coupling parameter at a fixed value of the bending rigidity $K/(k_B T) = 0.1$. Here we change χ over a range of six orders of magnitude spanning the transition from quenched to annealed regimes. The data exhibit a smooth crossover from the quenched area-scaling value (shown by a solid horizontal line) to the predicted annealed value (shown by a dashed horizontal line). The agreement is almost perfect at both converging ends within the statistical error-bars of the data (comparable to the symbol size, amounting to relative errors of about 2%). Note that in these regions of χ (e.g., for $\chi > 1$ or $\chi < 10^{-3}$), the data exhibit a very weak dependence on χ . As previously mentioned, this directly translates to a weak dependence of the ratio D/D_0 on the curvilinear diffusion coefficient, D_0 , when all other parameters are fixed (see Eq. (56)). In other words, in either limit $\chi \rightarrow 0$ or $\chi \rightarrow \infty$, D/D_0 depends only upon

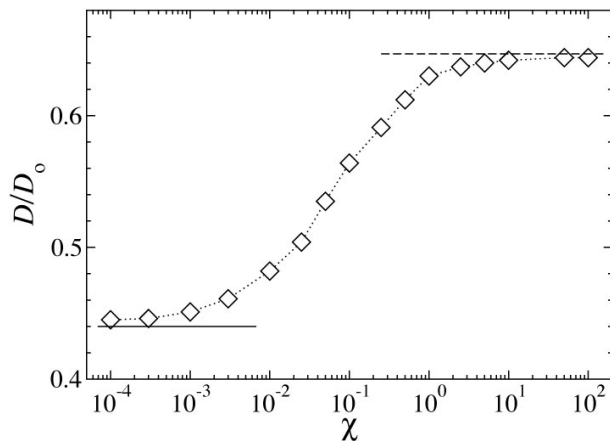


FIG. 12: Rescaled projected diffusion coefficient, D/D_0 , of a freely diffusing particle on a dynamically fluctuating elastic membrane as a function of the dynamical coupling parameter $\chi = k_B T / (4\eta D_0 L)$ at fixed membrane bending rigidity of $K/(k_B T) = 0.1$ for $M = 32$ and surface tension $\sigma = 0$. Symbols represent simulation data, the dashed horizontal line specifies the corresponding theoretical annealed value (Appendix B), while the solid line represents the quenched area-scaling value (dotted curve is guide to eyes). A smooth crossover is observed between the asymptotic annealed and quenched predictions. Error-bars are comparable to the symbol size.

the dimensionless parameters, $K/(k_B T)$ and M (as well as $\sigma L^2/(k_B T)$ when present). The practical definition of these limits is implied by the curve in Figure 12.

We find the same trend for all values of the bending rigidity as may be seen from Figure 11. Qualitatively, one can think of the χ value where D/D_0 reaches the mean value of the quenched and annealed predictions as a conventionally chosen crossover point beyond or below which the system is dominated by either quenched or annealed features as described in Section IV C 2. In Figure 12, this corresponds to a value of $\chi \sim 0.1$. For smaller bending rigidities, this crossover point tends to larger values of χ (as may already be seen from Figure 11), reflecting stronger quenched effects. A reverse trend is observed for larger bending rigidities.

F. Discussion of experimental systems

The following numbers represent typical values for integral membrane proteins diffusing in lipid bilayers [27] (but are specific to the case of diffusion of band 3 protein on the surface of the human red blood cell in the absence of osmotic stress and neglecting interactions with the cellular cytoskeleton [42]): $D_0 \simeq 0.5 \mu\text{m}^2/\text{s}$, $\eta = 0.06$ poise, $K/(k_B T) \simeq 5$ and $\sigma = 0$. For length scales around $2\pi q^{-1} = L \simeq 100$ nm, these numbers translate to $\chi \simeq 3$ and the time scale ratio (57) of $\tau_q^d/\tau_q^m \simeq 10^2$, which is close to the annealed limit. However, optical mea-

surements are limited to (at best) the diffraction limit of light, which is closer to $1 \mu\text{m}$ and cells are typically on the order of $10 \mu\text{m}$ or larger. For these larger membrane sizes of $L \simeq 1 - 10 \mu\text{m}$, one finds $\chi \simeq 0.3 - 0.03$ or the time scale ratio of $\tau_q^d/\tau_q^m \simeq 10 - 1$, which spans the intermediate regime. While some experimental systems may be adequately described by the annealed limit, other membrane systems, especially large ones, seem ill suited to such a description. The general results presented here will be of use in predicting D for systems outside the annealed and/or quenched regimes.

V. CONCLUSION AND DISCUSSION

We have analyzed the projected self-diffusion coefficient of a free Brownian particle on rough two-dimensional surfaces that may be static or fluctuating in time. This is achieved by establishing a position Langevin equation appropriate for particle diffusion on weakly curved membranes represented in Monge gauge. The Langevin equation implicitly incorporates curvature and gradient effects that hinder the diffusion of the particle once projected on a laboratory base plane. We have applied this equation numerically (using Brownian Dynamics simulation techniques) to several different examples of a static as well as a dynamic surface.

As shown, the dynamical state of the coupled particle-membrane system may be described by a dynamical coupling parameter, $\chi = k_B T / (4\eta L D_0)$ (with η being the medium viscosity, L the system size, and D_0 the particle curvilinear diffusion coefficient), that controls the separation of characteristic time scales for particle diffusion and membrane relaxation. Qualitatively, it represents the ratio between the relaxation time of membrane undulations of typical energy scale $k_B T$ and lateral range L to the time spent by the particle to diffuse over such a length scale. This parameter specifies the dynamical nature of surface disorder experienced by the diffusing particle with two well-defined limiting cases of quenched and annealed disorder being given by $\chi \rightarrow 0$ (static surface or fast diffusion) and $\chi \rightarrow \infty$ (fast-fluctuating surface or slow diffusion), respectively.

The simulation methods presented in this work enable one to study the diffusion process for the whole range of non-trivial intermediate couplings χ , where the membrane and particle diffusion time scales are comparable.

In all quenched cases considered here, we find that the simulation data are best described by the area-scaling prediction for the projected diffusion coefficient. Indeed, to within our statistical errors, the area-scaling result can be considered exact. The area-scaling prediction has so far been considered only as a plausible scaling result [16, 25] and no rigorous proof is available, to our knowledge, that demonstrates its validity in a systematic fashion. The variational bounds and the effective medium approximation discussed in detail in Ref. [16] show notable deviations from simulation data in all the studied

cases. The present findings call for a more detailed analysis of diffusion over two-dimensional surfaces, and in particular, an analytical explanation that can clarify the unanticipated success of area-scaling in the quenched disorder limit.

In view of the fact that many biological structures exhibit large static undulations (as in the endoplasmic reticulum [5] and the lateral cortex of auditory outer hair cells [27, 28]), it is important to realize that the annealed result may not be applied to these system. Area scaling provides the appropriate choice for D/D_0 .

In the annealed limit ($\chi \gg 1$), we have shown that the simulation data for the projected diffusion coefficient agree well with analytical annealed limiting results as calculated in Appendix B. The annealed diffusion coefficients are higher than the corresponding quenched values. This is more pronounced for strongly roughened membranes that may be represented by small bending rigidity (and surface tension). For vanishing bending rigidity, the annealed diffusion coefficient tends to $D/D_0 = 1/2$, whereas the corresponding quenched value tends to zero, reflecting a huge qualitative difference between the two in this limit. For large bending rigidities, the surface is almost planar and all different theoretical predictions converge to $D/D_0 = 1$, with deviations of only a few percent for $K/(k_B T) > 1$. This is why we have extensively studied the low bending rigidity regime in order to emphasize the physical mechanisms which affect the diffusion coefficient.

An important advantage of the present Langevin approach is that it can be easily generalized to include particle-particle and membrane-particle interactions (as in the case of active protein inclusions [48], where—unlike the present case—membrane dynamics are directly influenced by forces exerted by the proteins). This will enable numerical investigation of more complex and realistic models of biological membranes.

As a final note, we comment on some of the physics absent from the present study. This work considers the influence of surface shape on the diffusion process solely through the geometric effect of projection onto a base plane. We have neglected any effects whereby surface shape may alter the local character of the surface and the value of D_0 . For example, the curvature of a lipid bilayer may influence the value of D_0 itself [25] and we have neglected this effect. In the case of fluid lipid bilayers, it is clear that surface fluctuations must be accompanied by a local flow of lipids as membrane material is moved about. Such flows would be expected to drive particle motion and lead to correlations between membrane fluctuations and protein transport. Our study, and the others we are aware of [24, 25], completely neglect this effect. The problem of coupled fluctuations and hydrodynamic flow within the bilayer is a seemingly complex one, with only formal results available thus far [49].

Acknowledgments

We thank Hoda Boroudjerdi, David Dean, Nir Gov, Lawrence Lin and Phil Pincus for helpful discussions. This work was supported by the National Science Foundation (grant No. CHE-0321368 and grant No. CHE-0349196). F.B. is an Alfred P. Sloan Research Fellow and a Camille Dreyfus Teacher-Scholar.

Note Added in Proof

An interesting paper by Reister-Gottfried et al. [50] was published while this work was under review. That paper also considers the problem of diffusion over an annealed flexible membrane.

APPENDIX A: LANGEVIN EQUATION IN REDUCED REPRESENTATION

In this Appendix we derive the rescaled functions that enter in the rescaled Langevin equation for particle motion, Eq. (51). As explained in the text, this follows by simply plugging rescaled variables $\tilde{x} = x/L$, $\tilde{t} = D_0 t/L^2$ and $\tilde{h}(\tilde{x}, \tilde{y}, \tilde{t}) = h(x, y, t)/L$ into the actual Langevin equation (17) (or simply multiplying both sides of the equation by L/D_0). The rescaled drift, \tilde{v}_i , the rescaled multiplicative noise factor, $\tilde{\tau}_{ij}$ (being the square-root of the inverse metric tensor, Eq. (21)), may thus be obtained as

$$\tilde{v}_i[\tilde{h}(\{\tilde{x}_k\}, \tilde{t})] = \frac{L}{D_0} v_i, \quad \tilde{\tau}_{ij}[\tilde{h}(\{\tilde{x}_k\}, \tilde{t})] = \tau_{ij}, \quad (\text{A1})$$

where we have explicitly indicated their dependence on space coordinates (particle position) through the surface height profile, $h(\{x_k\}, t) = h(x, y, t)$ (for $i, j, k = 1, 2$ in 2D). It is to be noted that the metric tensor g_{ij} , and therefore its inverse, $(\mathbf{g}^{-1})_{ij}$, and determinant, g , remain invariant under rescaling coordinates, e.g., $g_{ij} = \tilde{g}_{ij} \equiv \delta_{ij} + \tilde{\partial}_i \tilde{h} \tilde{\partial}_j \tilde{h}$, where $\tilde{\partial}_i \equiv \partial/\partial \tilde{x}_i$. Hence using Eqs. (18) and (21) we have

$$\tilde{v}_i = - \left[(\mathbf{g}^{-1})_{jk} \tilde{\partial}_j \tilde{\partial}_k \tilde{h} \right] \frac{\tilde{\partial}_i \tilde{h}}{g}, \quad (\text{A2})$$

$$\tilde{\tau}_{ij} = \delta_{ij} - \frac{\tilde{\partial}_i \tilde{h} \tilde{\partial}_j \tilde{h}}{g + \sqrt{g}}. \quad (\text{A3})$$

Likewise, the noise term, $\eta_i(t)$, in Eq. (17) is rescaled as $\tilde{\eta}_i(\tilde{t}) = L\eta_i(t)/D_0$. Therefore, $\tilde{\eta}_i(\tilde{t})$ is a Gaussian white noise with zero mean, $\langle \tilde{\eta}_i(\tilde{t}) \rangle = 0$, and variance $\langle \tilde{\eta}_i(\tilde{t}) \tilde{\eta}_j(\tilde{t}') \rangle = 2\delta_{ij} \delta(\tilde{t} - \tilde{t}')$.

A similar scheme can be used to rescale the membrane dynamical equation (48) as explained in the text. In this case, the rescaled noise term, $\tilde{\xi}_{\mathbf{q}}(\tilde{t})$, in Eq. (52) is related to the actual noise term, $\xi_{\mathbf{q}}(t)$, in Eq. (48), via $\tilde{\xi}_{\mathbf{q}}(\tilde{t}) = L\xi_{\mathbf{q}}(t)/\sqrt{D_0}$. Therefore, $\tilde{\xi}_{\mathbf{q}}(\tilde{t})$ is a Gaussian

white noise with $\langle \tilde{\xi}_{\mathbf{q}}(\tilde{t}) \rangle = 0$ and variance $\langle \tilde{\xi}_{\mathbf{q}}(\tilde{t}) \tilde{\xi}_{\mathbf{q}'}(\tilde{t}') \rangle = 2\delta_{\mathbf{q},-\mathbf{q}'} \delta(\tilde{t} - \tilde{t}')$.

APPENDIX B: THEORETICAL ANNEALED PREDICTION FOR THE RATIO D/D_0

As originally shown by Gustafsson et al. [16], the diffusion coefficient ratio D/D_0 for a free particle diffusing on a fast-fluctuating surface is given by

$$\frac{D}{D_0} \Big|_{\text{annealed}} = \frac{1}{2} \left(1 + \left\langle \frac{1}{g} \right\rangle_h \right), \quad (\text{B1})$$

which has a form similar to the upper bound in the quenched limit, Eq. (31), but here brackets denote an ensemble average over equilibrium configurations of the surface as will be specified below. Gustafsson et al. [16] calculated this average for a generic *infinite* surface exhibiting an isotropic Gaussian distribution of surface gradients, ∇h (and thus a scalar diffusion coefficient). For an elastic membrane of arbitrary size L (and finite small-scale cut-off, a), the gradient distribution is in general anisotropic. In this Appendix, we demonstrate how the ensemble average in Eq. (B1) can be calculated for this latter case.

The ensemble average of any function, $Q(\nabla h(\boldsymbol{\rho}))$, of surface height gradient, ∇h , at a given point $\boldsymbol{\rho} = (x, y)$, can be expressed as a functional integral over equilibrium membrane configurations as

$$\langle Q(\nabla h(\boldsymbol{\rho})) \rangle_h = \int \frac{\mathcal{D}[h(\boldsymbol{\rho}')] }{\mathcal{Z}_h} Q(\nabla h(\boldsymbol{\rho})) e^{-\beta \mathcal{H}[h(\boldsymbol{\rho}')]} , \quad (\text{B2})$$

where $\beta = 1/(k_B T)$ and $\mathcal{Z}_h = \int \mathcal{D}[h] \exp[-\mathcal{H}/(k_B T)]$ is the membrane partition function. An example for Q is the quantity $1/g$ appearing in Eq. (B1), where $g \equiv 1 + (\nabla h)^2$. Denoting statistically probable values of ∇h by \mathbf{u} , we obtain a formally equivalent expression for $\langle Q \rangle_h$ at a given point $\boldsymbol{\rho}$, i.e.

$$\langle Q \rangle_h = \int d\mathbf{u} Q(\mathbf{u}; \boldsymbol{\rho}) P_u(\mathbf{u}; \boldsymbol{\rho}), \quad (\text{B3})$$

where

$$P_u(\mathbf{u}; \boldsymbol{\rho}) = \int \frac{\mathcal{D}[h(\boldsymbol{\rho}')]}{\mathcal{Z}_h} \delta(\mathbf{u} - \nabla h(\boldsymbol{\rho})) e^{-\beta \mathcal{H}[h(\boldsymbol{\rho}')]} \quad (\text{B4})$$

$$= \left\langle \delta(\mathbf{u} - \nabla h(\boldsymbol{\rho})) \right\rangle_h, \quad (\text{B5})$$

is nothing but the probability distribution function of the height gradient, $\mathbf{u} = \nabla h$, at position $\boldsymbol{\rho}$. We thus first need to determine $P_u(\mathbf{u}; \boldsymbol{\rho})$ in order to calculate Eq. (B1).

We proceed by replacing the delta-function in Eq. (B4) by its Fourier representation, i.e.

$$\delta(\mathbf{u} - \nabla h(\boldsymbol{\rho})) = \int \frac{d\boldsymbol{\mu}}{(2\pi)^2} \exp \left[i\boldsymbol{\mu} \cdot (\mathbf{u} - \nabla h(\boldsymbol{\rho})) \right], \quad (\text{B6})$$

where $\boldsymbol{\mu}$ is a Fourier conjugate of \mathbf{u} . Inserting this into Eq. (B4) and using the explicit form of the Hamiltonian (37) (in Fourier representation), we reach at the following expression

$$P_u(\mathbf{u}; \boldsymbol{\rho}) = \int \frac{d\boldsymbol{\mu}}{(2\pi)^2} e^{i\boldsymbol{\mu} \cdot \mathbf{u}} \mathcal{I}(\boldsymbol{\mu}; \boldsymbol{\rho}), \quad (\text{B7})$$

with $\mathcal{I}(\boldsymbol{\mu}; \boldsymbol{\rho})$ being the so-called generating function of height-gradient moments, which is obtained as

$$\mathcal{I}(\boldsymbol{\mu}; \boldsymbol{\rho}) = \int \frac{\mathcal{D}h_{\mathbf{q}}}{\mathcal{Z}_h} e^{-\frac{1}{2L^2} \sum_{\mathbf{q}} (\beta \Omega_{\mathbf{q}} |h_{\mathbf{q}}|^2 - 2\boldsymbol{\mu} \cdot \mathbf{q} e^{i\mathbf{q} \cdot \boldsymbol{\rho} h_{\mathbf{q}}})}, \quad (\text{B8})$$

where $\mathcal{D}h_{\mathbf{q}} = \prod_{\mathbf{q}} dh_{\mathbf{q}}$ and $\Omega_{\mathbf{q}} = Kq^4 + \sigma q^2$. The above Gaussian integral can be evaluated and it follows that the dependence on the position of the generating function, \mathcal{I} , drops out yielding

$$\mathcal{I}(\boldsymbol{\mu}; \boldsymbol{\rho}) = \mathcal{I}(\boldsymbol{\mu}) = \exp \left[-\frac{1}{2\beta L^2} \sum_{\mathbf{q}} \frac{(\mathbf{q} \cdot \boldsymbol{\mu})^2}{\Omega_{\mathbf{q}}} \right]. \quad (\text{B9})$$

Putting this expression into Eq. (B7), one finds after taking the Gaussian integral over $\boldsymbol{\mu}$ that

$$P_u(\mathbf{u}; \boldsymbol{\rho}) = P_u(\mathbf{u}) = \frac{e^{-\frac{1}{2} \mathbf{u} \cdot \hat{\mathbf{A}}^{-1} \cdot \mathbf{u}}}{2\pi \sqrt{\det \hat{\mathbf{A}}}}, \quad (\text{B10})$$

where the elements of the 2×2 matrix $\hat{\mathbf{A}}$ read

$$(\hat{\mathbf{A}})_{ij} \equiv \langle \partial_i h \partial_j h \rangle = \frac{1}{\beta L^2} \sum_{\mathbf{q}} \frac{q_i q_j}{\Omega_{\mathbf{q}}}. \quad (\text{B11})$$

In the limit of large membrane size $M = L/a \rightarrow \infty$, the cross terms (off-diagonal elements) of $\hat{\mathbf{A}}$ vanish leading to isotropic height-gradient probability distribution used in Ref. [16], i.e.

$$P_u(\mathbf{u}) \rightarrow \frac{1}{\pi u^2} e^{-u^2/\bar{u}^2} \quad (\text{B12})$$

with the variance defined as $\bar{u}^2 = \langle (\nabla h)^2 \rangle$.

For a finite $M = L/a$, one can calculate desirable averages, Eq. (B3), using the anisotropic height-gradient distribution (B10). For the particular case of $\langle 1/g \rangle_h$ in Eq. (B1), the computations need to be carried out numerically. The results for the predicted annealed ratio D/D_0 , Eq. (B1), at different bending rigidities (and zero surface tension) are shown in Figures 11 and 12 (dashed lines). (Note that the annealed expression for D in general involves additional ‘‘off-diagonal’’ terms containing cross-correlation functions, but they are negligible for the membrane size chosen here—see Appendix C and Ref. [24].)

Reister et al. [24] present a method to explicitly evaluate Eq. (B1) for an elastic membrane, but their scheme actually computes $\langle \mathcal{A}_{\perp} / (\int d^2x g) \rangle_h$ instead of $\langle 1/g \rangle_h$, which in principle represents a different quantity. The results reported in Ref. [24] underestimate the annealed values of D/D_0 by up to 5-10% depending on the bending rigidity (with the larger errors being where the discrete summation over \mathbf{q} -modes is approximated by an integral).

APPENDIX C: ANNEALED LIMIT: ADIABATIC ELIMINATION OF FAST VARIABLES

The coupled membrane-particle dynamical equations (51) and (52) as represented in rescaled units provide an appropriate analytical framework for a systematic perturbative analysis around the annealed-disorder limit. The time-scale separation in this limit is such that the membrane degrees of freedom represent the fast variables, whereas the particle degrees of freedom constitute the slow variables in the system. Under this condition, one can use the methods described in literature to adiabatically eliminate the fast variables and derive effective dynamical equations for the slow ones.

Equations (51) and (52) already indicate how this procedure should be done in the present context by making use of χ as an expansion parameter. Following Risken [3], we can develop a perturbative scheme much in the spirit of Born-Oppenheimer approximation. The Fokker-Planck equation for the joint probability distribution of the set of variables $\{\tilde{x}_{\mathbf{q}}(\tilde{t}), \tilde{x}_i(\tilde{t})\}$ may be written as

$$\dot{\tilde{P}}(\{\tilde{x}_i, \tilde{h}_{\mathbf{q}}\}, \tilde{t}) = (\hat{O}_x + \chi \hat{O}_h) \tilde{P}(\{\tilde{x}_i, \tilde{h}_{\mathbf{q}}\}, \tilde{t}), \quad (\text{C1})$$

where the Fokker-Planck operators associated with x - and h -variables read

$$\hat{O}_x = -\frac{\partial}{\partial \tilde{x}_i} \tilde{v}_i + \frac{\partial^2}{\partial \tilde{x}_i \partial \tilde{x}_j} (\mathbf{g}^{-1})_{ij} \quad (\text{C2})$$

$$\hat{O}_h = \sum_{\mathbf{q}} \left(\tilde{\omega}_{\mathbf{q}} \frac{\partial}{\partial \tilde{h}_{\mathbf{q}}} \tilde{h}_{\mathbf{q}} + \tilde{\Lambda}_{\mathbf{q}} \frac{\partial^2}{\partial \tilde{h}_{\mathbf{q}} \partial \tilde{h}_{-\mathbf{q}}} \right). \quad (\text{C3})$$

The idea here is to expand $\tilde{P}(\{\tilde{x}_i, \tilde{h}_{\mathbf{q}}\}, \tilde{t})$ in terms of the eigen-functions of the operator \hat{O}_h (which are in the present context independent of $\{\tilde{x}_i\}$), i.e.

$$\tilde{P}(\{\tilde{x}_i, \tilde{h}_{\mathbf{q}}\}, \tilde{t}) = \sum_{m=0}^{\infty} c_m(\{\tilde{x}_i\}, \tilde{t}) \phi_m(\{\tilde{h}_{\mathbf{q}}\}). \quad (\text{C4})$$

Here we have assumed that a stationary solution as well as a discrete spectrum of eigen-functions, $\phi_n(\{\tilde{h}_{\mathbf{q}}\})$ (with $n \geq 0$), exist, i.e.

$$\hat{O}_h \phi_n(\{\tilde{h}_{\mathbf{q}}\}) = -\lambda_n \phi_n(\{\tilde{h}_{\mathbf{q}}\}), \quad (\text{C5})$$

with $\lambda_0 = 0$ being the stationary solution corresponding to the equilibrium distribution function of membrane, $\phi_0(\{\tilde{h}_{\mathbf{q}}\}) = \prod_{\mathbf{q}} \tilde{P}_{\text{eq}}(\tilde{h}_{\mathbf{q}})$. Note that \tilde{P}_{eq} is given by Eq.

(55). Inserting Eq. (C4) into the joint Fokker-Planck equation (C1), one finds

$$\left(\frac{\partial}{\partial \tilde{t}} + \chi \lambda_n \right) c_n = \sum_{m=0}^{\infty} \mathcal{L}_{nm} c_m, \quad (\text{C6})$$

where $\mathcal{L}_{nm}(\{\tilde{x}_i\}) = \int \mathcal{D}\tilde{h}_{\mathbf{q}} \phi_n^\dagger \hat{O}_x \phi_m$ with ϕ_n^\dagger being the eigen-function of the adjoint operator \hat{O}_h^\dagger , which is needed since the Fokker-Planck operator is non-Hermitian [3].

For large $\chi \gg 1$, the time derivative may be neglected in Eq. (C6) for $n \geq 1$ in the long-time limit $\tilde{t} \gg (\chi \lambda_1)^{-1}$, and only kept in the equation governing c_0 (with $\lambda_0 = 0$). By doing so, one can easily derive a perturbative expression for the latter equation. But it turns out that c_0 is nothing but the time-dependent probability distribution of the slow variable averaged over the fast-variable distribution [3], i.e., $c_0 = \tilde{\mathcal{P}}(\{\tilde{x}_i\}, \tilde{t}) = \int \mathcal{D}\tilde{h}_{\mathbf{q}} \tilde{P}(\{\tilde{x}_i, \tilde{h}_{\mathbf{q}}\}, \tilde{t})$. Therefore, one ends up with the desired effective equation governing the probability distribution of particle position on a fast-fluctuating membrane, which admits the following perturbative form

$$\dot{\tilde{\mathcal{P}}}(\{\tilde{x}_i\}, \tilde{t}) = \left(\hat{O}_x^{(0)} + \chi^{-1} \hat{O}_x^{(1)} + \mathcal{O}(\chi^{-2}) \right) \tilde{\mathcal{P}}(\{\tilde{x}_i\}, \tilde{t}), \quad (\text{C7})$$

with the zeroth-order term being given by

$$\hat{O}_x^{(0)} \equiv \mathcal{L}_{00}(\{\tilde{x}_i\}) = -\frac{\partial}{\partial \tilde{x}_i} \langle \tilde{v}_i \rangle_h + \frac{\partial^2}{\partial \tilde{x}_i \partial \tilde{x}_j} \langle (\mathbf{g}^{-1})_{ij} \rangle_h, \quad (\text{C8})$$

where the drift, $\langle \tilde{v}_i \rangle_h$, and the inverse metric tensor (rescaled diffusion matrix), $\langle (\mathbf{g}^{-1})_{ij} \rangle_h$, are averaged over the equilibrium distribution function of membrane height at a given point as, e.g., defined in Eq. (B2). The first-order operator in Eq. (C7) reads $\hat{O}_x^{(1)} = \sum_{n=1}^{\infty} \mathcal{L}_{0n}(\{\tilde{x}_i\}) \mathcal{L}_{n0}(\{\tilde{x}_i\}) / \lambda_n$.

Note that the zeroth-order term in Eq. (C7) becomes *exact* in the annealed limit $\chi \rightarrow \infty$. Using explicit expressions given before for \tilde{v}_i and $(\mathbf{g}^{-1})_{ij}$ (and neglecting small off-diagonal terms for large L), the annealed expression for D/D_0 , Eq. (B1), immediately follows. The effective Fokker-Planck equation for particle diffusion on an annealed surface was first derived in Ref. [24] using a pre-averaging approximation, which gives the effective Fokker-Planck equation (C7) up to the zeroth-order term. The preceding derivation places this result within a systematic framework and predicts higher-order corrections.

[1] J. Crank, *The Mathematics of Diffusion* (Oxford University Press, New York, 1992)
 [2] H.C. Berg, *Random Walks in Biology* (Princeton University Press, Princeton, 1993)
 [3] H. Risken, *The Fokker-Planck Equation* (Springer-Verlag, Berlin, 1996)

[4] N.G. van Kampen, *Stochastic Processes in Physics and Chemistry* (North-Holland, Amsterdam, 1992)
 [5] B. Alberts et al., *Molecular Biology of the Cell* (Garland Publishing, New York, 1994)
 [6] H.C. Berg, E.M. Purcell, *Biophys. J.* **20**, 193 (1977)
 [7] S.J. Singer, G.L. Nicolson, *Science* **175**, 720 (1972)

- [8] R. Lipowsky, E. Sackmann (Eds.), *Structure and Dynamics of Membranes* (Elsevier, Amsterdam, 1995)
- [9] K. Jacobson, E.D. Sheets, R. Simson, *Science* **268**, 1441 (1995)
- [10] M.J. Saxton, K. Jacobson, *Annu. Rev. Biophys. Biomol. Struct.* **26**, 373 (1997)
- [11] D. Axelrod et al., *Biophys. J.* **16**, 1055 (1976)
- [12] B. Halle, S. Gustafsson, *Phys. Rev. E* **56**, 690 (1997)
- [13] F. Zhang, G.M. Lee, K. Jacobson, *BioEssays* **15**, 579 (1993)
- [14] P.G. Saffman, M. Delbrück, *Proc. Natl. Acad. Sci.* **72**, 3111 (1975)
- [15] D.M. Broday, *Bulletin Math. Biol.* **64**, 531 (2002)
- [16] S. Gustafsson, B. Halle, *J. Chem. Phys.* **106**, 1880 (1997)
- [17] B. Halle, S. Gustafsson, *Phys. Rev. E* **55**, 680 (1997)
- [18] R. Holyst, D. Plewczynski, A. Aksimentiev, *Phys. Rev. E* **60**, 302 (1999); D. Plewczynski, R. Holyst, *J. Chem. Phys.* **113**, 9920 (2000)
- [19] J. Faraudo, *J. Chem. Phys.* **116**, 5831 (2002)
- [20] M. Christensen, *J. Comp. Phys.* **201**, 421 (2004)
- [21] J.L. Jackson, S.R. Coriell, *J. Chem. Phys.* **38**, 959 (1963)
- [22] R. Festa, E.G. d'Agliano, *Physica* **90A**, 229 (1978)
- [23] M. King, *J. Theor. Biol.* **227**, 323 (2004)
- [24] E. Reister, U. Seifert, *Europhys. Lett.* **71**, 859 (2005)
- [25] N.S. Gov, *Phys. Rev. E* **73**, 041918 (2006)
- [26] I.F. Sbalzarini, A. Hayer, A. Helenius, P. Koumoutsakos, *Biophys. J.* **90**, 878 (2006)
- [27] D. Boal, *Mechanics of the Cell* (Cambridge University Press, New York, 2002)
- [28] C.A. Smith, *Adv. Sci.* **24**, 419 (1968); M. Ulfendahl, N. Slepecky, *J. Submicrosc. Cytol. Pathol.* **20**, 47 (1988)
- [29] S.T. Milner, S.A. Safran, *Phys. Rev. A* **36**, 4371 (1987)
- [30] F. Brochard, J. F. Lennon, *J. Phys. (Paris)* **36**, 1035 (1975)
- [31] I.M. Sokolov, *Short Reports in Physics (Moscow)* **8**, 17 (1987)
- [32] Since persistence lengths of typical biomembranes are much larger than cellular dimensions [8, 27], it is completely natural to assume a membrane surface without overhangs and hence a single-valued $h(x, y)$.
- [33] An introduction to differential geometry accessible to a chemical physics audience may be found in Ref. [43]; see also R.D. Kamien, *Rev. Mod. Phys.* **74**, 953 (2002) and L.P. Eisenhart, *Riemannian Geometry* (Princeton University Press, Princeton, 1926) for more advanced presentations.
- [34] For the sake of presentation, we do not distinguish between co- and contra-variant variables in our notation.
- [35] C.W. Gardiner, *Handbook of Stochastic Methods* (Springer-Verlag, Berlin, 2004)
- [36] Note that $\tau = (\mathbf{g}^{-1})^{1/2}$ may be written in a symmetric fashion as $\tau = \mathbf{S}\mathbf{\Lambda}^{1/2}\mathbf{S}^T$, where \mathbf{S} is the eigen-vector matrix of the positive-definite inverse metric tensor \mathbf{g}^{-1} , and $\mathbf{\Lambda}$ its diagonal eigen-value matrix, both of which can be calculated explicitly in Monge gauge using Eq. (4).
- [37] J. Zinn-Justin, *Quantum Field Theory and Critical Phenomena* (Oxford University Press, Oxford, 2002)
- [38] D.L. Ermak, J.A. McCammon, *J. Chem. Phys.* **69**, 1352 (1978)
- [39] Lord Rayleigh, *Nature* **95**, 66 (1915); E. Buckingham, *Phys. Rev.* **4**, 345 (1914)
- [40] H. Flyvberg, H.G. Petersen, *J. Chem. Phys.* **91**, 461 (1989)
- [41] T.C. Peteson et al., *Phys. Rev. B* **72**, 125417 (2005)
- [42] L. C.-L. Lin, F.L.H. Brown, *Phys. Rev. Lett.* **93**, 256001 (2004); *Phys. Rev. E* **72**, 011910 (2005); *Biophys. J.* **86**, 764 (2004)
- [43] S.A. Safran, *Statistical Thermodynamics of Surfaces, Interfaces and Membranes* (Westview Press, Boulder, 1994)
- [44] P.C. Hohenberg, B.I. Halperin, *Rev. Mod. Phys.* **49**, 435 (1977)
- [45] M. Doi, S.F. Edwards, *The Theory of Polymer Dynamics* (Oxford University Press, New York, 1986)
- [46] L. C.-L. Lin, F.L.H. Brown, *J. Chem. Theory Comput.* **2**, 472 (2006)
- [47] J. Prost, R. Bruinsma, *Europhys. Lett.* **33**, 321 (1996)
- [48] L. C.-L. Lin, N. Gov, F.L.H. Brown, *J. Chem. Phys.* **124**, 074903 (2006)
- [49] W. Cai, T.C. Lubensky, *Phys. Rev. Lett.* **73**, 1186 (1994); *Phys. Rev. E* **52**, 4251 (1995)
- [50] E. Reister-Gottfried, S.M. Leitenberger, U. Seifert, *Phys. Rev. E* **75**, 011908 (2007)